Polynomial chaos expansion for permutation and cyclic permutation invariant systems: application to mistuned bladed disks

Juliette Dréau, Benoit Magnain, Florence Nyssen, Alain Batailly

POLYTECHNIQUE MONTRÉAL
UNIVERSITÉ D'INGÉNIERIE

LABORATOIRE D'ANALYSE VIBRATOIRE ET ACOUSTIQUE

Polynomial chaos expansion for permutation and cyclic permutation invariant systems: Application to mistuned bladed disks

Juliette Dréau[1], Benoit Magnain[2], Florence Nyssen[1], and Alain Batailly[1]

Abstract

This article deals with the stochastic modeling of industrial mistuned bladed disks. More specifically, a cost-efficient implementation of polynomial chaos expansion is proposed, it is dedicated to mathematical systems exhibiting permutation invariance or cyclic permutation invariance of their random variables. Significant gains are obtained in comparison to the classical implementation of polynomial chaos expansion since potentially costly evaluations of the investigated deterministic system are only required over a small subspace of the random space. The proposed methodology is detailed and validated on analytical test cases before it is applied to two mistuned bladed disks models. First, computations carried out with a simplified bladed disk model allow an in-depth comparison between Monte Carlo simulations, previously published results with a standard polynomial chaos expansion and the proposed methodology. The latter is then employed to assess the influence of mistuning on the eigenfrequencies and amplification magnification of an industrial compressor stage. It is evidenced that in comparison to the standard polynomial chaos expansion, the proposed methodology yields computational gains of the same order of magnitude as the ones obtained going from Monte Carlo simulations to polynomial chaos expansion. Alternately, the proposed methodology may be employed to significantly increase the accuracy of the standard polynomial chaos expansion while featuring an identical computational cost.

Keywords

mistuning; bladed disk; polynomial chaos expansion; cyclic permutation invariance; vibration amplification; uncertainty quantification

1 - Département de génie mécanique, École Polytechnique de Montréal, Montréal, H3T 1J4, Canada,
2 - LaMé, EA 7494, INSA CVL, Univ. Orléans, Univ. Tours, F-18020, Bourges Cedex, France

Méthode du chaos polynomial pour les systèmes invariants par permutation et par permutation circulaire: Application aux désaccordages des roues aubagées

Juliette Dréau[1], Benoit Magnain[2], Florence Nyssen[1], et Alain Batailly[1]

Résumé

Cet article porte sur la modélisation stochastique de roues aubagées industrielles désaccordées. Plus précisément, une implémentation peu coûteuse de la méthode du chaos polynomial est proposée, celle-ci est dédiée aux systèmes mathématiques présentant une invariance par permutation ou une invariance par permutation circulaire de leurs variables aléatoires. Des gains significatifs sont obtenus par rapport à l'implémentation classique de la méthode du chaos polynomial puisque des évaluations potentiellement coûteuses du système déterministe étudié ne sont nécessaires que sur un petit sous-espace de l'espace aléatoire. La méthodologie proposée est détaillée et validée sur des cas tests analytiques avant d'être appliquée à deux modèles de roues aubagées désaccordées. Tout d'abord, les calculs effectués avec un modèle simplifié de roue aubagée permettent une comparaison approfondie entre les simulations de Monte-Carlo, les résultats publiés précédemment avec la méthode du chaos polynomial standard et la méthodologie proposée. Cette dernière est ensuite utilisée pour évaluer l'influence du désaccordage sur les fréquences propres et le facteur d'amplification d'un étage de compresseur industriel. Il est prouvé que par rapport à la méthode du chaos polynomial standard, la méthodologie proposée fournit des gains de calcul de même qualité que ceux obtenus en procédant à des simulations de Monte-Carlo et en utilisant la méthode du chaos polynomial standard. La méthodologie proposée peut également être utilisée pour augmenter de manière significative la précision de la méthode du chaos polynomial standard tout en présentant un coût de calcul identique.

Mots-clés

désaccordage; roue aubagée; méthode du chaos polynomial; invariance par permutation circulaire; amplification des vibrations; calcul d'incertitude

1 - Département de génie mécanique, École Polytechnique de Montréal, Montréal, H3T 1J4, Canada,
2 - LaMé, EA 7494, INSA CVL, Univ. Orléans, Univ. Tours, F-18020, Bourges Cedex, France

1 Introduction

The design of bladed disks, which are key components of any aircraft engine or gas turbine system, has been the focus of a broad spectrum of research works over the past decades [1, 2]. Putting aside all the research efforts related to the design of aerodynamically efficient blade profiles [3], there have been several structural dynamics related challenges [4, 5] that designers and researchers had to tackle to build more efficient aircraft engines with a reduced environmental footprint. In particular, unavoidable imperfections in terms of material properties homogeneity and manufacturing tolerances [6, 7], which translate into small blade-to-blade mechanical behavior differences, break the bladed disk cyclic symmetry. This phenomenon, known as small mistuning [8], yields energy localization [9, 10] and vibration amplifications [11, 12] that may be detrimental to the bladed disk lifespan [13]. For this reason, the topic of energy dissipation has been at the heart of many research programs for safer aircraft engines [14, 15]. Beside of small mistuning, large mistuning—which is often related to accidental configurations, for instance due to blade damage [4]—has also been a widely investigated topic [16, 17]. In the present article, the focus is made on non-accidental configurations and only small mistuning is considered. For the sake of readability, it is hereafter simply referred to as mistuning.

While mistuning was first investigated on simplified phenomenological or analytical models [18], the need for accurate predictions of vibration amplifications drove the development of sophisticated modeling techniques in order to efficiently account for it in high fidelity tri-dimensional finite element models [4, 5]. In addition to the modeling challenge, the inherently random nature of mistuning implies that it has typically been analyzed considering a stochastic framework [19, 20, 21, 22]. As a consequence, classical Monte Carlo simulations (MCS) have been the numerical workhorse of a large amount of studies [12]. However, there exists alternative approaches such as spectral methods [23], including the well-known Polynomial Chaos Expansion (PCE) [24] which became increasingly popular over the last decade. PCE-based numerical approaches may be intrusive [25] or non-intrusive [26], the latter being more commonly considered for the analysis of large industrial mechanical systems [27, 28].

So far, research investigations on mistuning mostly took place within a structurally linear framework [29, 20]. The analysis of mistuned bladed disks in a nonlinear context is a very recently open research question [30, 31]. It has been driven by the fact that aircraft engine designers cannot neglect anymore the influence of nonlinear phenomena that arise at certain interfaces, such as friction damping at the blade/disk interface [32, 33, 34] or structural contacts at the blade-tip/casing interface [35, 36, 37]. Besides the theoretical challenges inherent to the treatment of the nonlinear interfaces [38], there is a significant computational cost to combining nonlinear structural phenomena and mistuning to a point where Monte Carlo simulations may yield cumbersome computation times: with current computing hardware, weeks or months of calculations may be required for some applications [39]. In this context, there is a need for the development of efficient numerical methodologies propitious to the combined analysis of nonlinear structural interactions and mistuning.

PCE has been applied to many different types of applications [40, 41]. However, for sophisticated engineering applications, potentially exhibiting a nonlinear mechanical behavior, one may consider two types of limitations of this methodology. Firstly, by default, PCE relies on continuous smooth polynomial functions that may be ill-suited for the description of certain types of nonlinearities [42]. Secondly, for sophisticated problems, it may be required to increase the degree of the polynomial interpolation so as to accurately capture its mechanical behavior. This implies a very significant increase in the number of required evaluations of the deterministic mechanical problem in order to build the interpolation, also known as the curse of dimensionality, to a point where the number of evaluations may reach a similar number than the one required for Monte Carlo simulations. Several solutions have been proposed in the literature to mitigate both issues. Notably, there has been a significant amount of research focusing on piecewise PCE [42] for a variety of nonlinear problems [43]. In addition, numerical techniques have been proposed to reduce the number of required evaluations [44, 45].

Nonetheless, in the field of turbomachinery, when modeling mistuning or blade specific parameters on a large bladed disk—that may easily feature more than twenty blades—a very large number of random variables must be considered which severely constrains the degree of the polynomial interpolation to low values [41, 2]. This comes at the cost of less accurate results and thus constitutes a bottleneck for a widespread application of PCE in the field of turbomachinery.

Building on an observation made in the context of the implementation of an intrusive PCE for the prediction of

amplifications in phenomenological mistuned bladed disks [46], this study focuses on an evolution of non-intrusive PCE for cyclically symmetric mechanical systems that yields a significant increase in terms of computational efficiency. It relies on the idea that the underlying mathematical model used for the analysis of bladed disk mistuning is cyclic permutation invariant.

In the first section of the article, the theoretical foundation of PCE is recalled for the sake of completeness. The proposed developments are then detailed in the second section of the article which is divided within two subsections: the first one focuses on permutation invariant systems while the second one more specifically deals with cyclic permutation invariant systems. For each type of system, mathematical demonstrations are provided along with a detailed validation of the methodology on analytical test functions. Finally, in the third section of the article, the proposed methodology is applied to a phenomenological bladed disk, similar to the one used in [46], and to a 3D industrial finite element compressor stage model.

2 Polynomial chaos expansion

Polynomial chaos expansion introduced by Weiner [24] is based on the expansion of the response Y of a stochastic system, of finite variance, into a series of orthogonal polynomials. Initially established for random variables of normal distribution, the expansion was based on multivariate Hermite polynomials for which the convergence of the series is ensured by the theorem of Cameron-Martin [47]. The scope of the method was then extended to different probability distributions by Xiu and Karniadakis [48]. Their researches have identified the family of polynomials to be used according to the probability distribution of each of the system's random variables in order to ensure an exponential convergence of the series: this is usually referred to as the Askey scheme [48].

2.1 Theoretical formulation

In this section, the investigated system features m_s independent random variables $\mathbf{X} = [X_1, \dots, X_{m_s}]$, and its response is denoted $Y(\mathbf{X})$. As an example, when considering an aircraft engine bladed disk, the random variables X_k and the system response Y may respectively stand for the blades' stiffness and the maximal vibration amplitude for a given excitation force. Following the Askey scheme, a change of the X_k variable to a reduced random variable ξ_k, *e.g.* to standard normal variables for normal distribution, is performed by an isoprobabilistic transformation T_k in such a way that:

$$X_k = T_k(\xi_k). \tag{1}$$

The probability density function of each random variable ξ_k is denoted by f_{ξ_k} and the vector of reduced variables is denoted by $\boldsymbol{\xi} = [\xi_1, \dots, \xi_{m_s}]$.

PCE consists in computing the coefficients $a_{\boldsymbol{\alpha}}$, also called stochastic modes or PCE coefficients, so that the system response Y is written as:

$$Y(\boldsymbol{\xi}) = \sum_{\boldsymbol{\alpha} \in \mathbb{N}^{m_s}} a_{\boldsymbol{\alpha}} \Psi_{\boldsymbol{\alpha}}(\boldsymbol{\xi}), \tag{2}$$

where the multivariate polynomials $\Psi_{\boldsymbol{\alpha}}$ constitute the PCE basis, and $\boldsymbol{\alpha} = [\alpha_1, \dots, \alpha_{m_s}]$ is a vector of multi-index. The multivariate polynomials are defined by the product of univariate polynomials Φ_{α_k} of degree α_k:

$$\Psi_{\boldsymbol{\alpha}}(\boldsymbol{\xi}) = \prod_{k=1}^{m_s} \Phi_{\alpha_k}(\xi_k). \tag{3}$$

Depending on the probability distribution of ξ_k, the polynomial Φ_{α_k} is chosen according to the family of polynomials identified by the Askey scheme. The polynomials of the PCE basis are orthonormalized as follows:

$$< \Psi_{\boldsymbol{\alpha}}, \Psi_{\boldsymbol{\beta}} >= \prod_{k=1}^{m_s} \int_{\mathbb{R}} \Phi_{\alpha_k}(x) \Phi_{\beta_k}(x) f_{\xi_k}(x) dx = \prod_{k=1}^{m_s} \delta_{\alpha_k \beta_k}, \tag{4}$$

where $\delta_{\alpha_k \beta_k}$ is the Kronecker symbol.

In practice, the PCE expansion is limited to a finite number of terms by truncation. For a maximum degree q, this truncation consists in selecting all polynomials $\Psi_{\boldsymbol{\alpha}}$ of degree lower or equal to q by using the truncation set $\mathcal{A}$:

$$\mathcal{A} = \{\boldsymbol{\alpha} \in \mathbb{N}^{m_s}, |\boldsymbol{\alpha}| = \sum_{k=1}^{m_s} \alpha_k \leq q\}. \tag{5}$$

This set is the disjoint union of the sets $\mathcal{A}_i = \{\boldsymbol{\alpha} \in \mathbb{N}^{m_s}, |\boldsymbol{\alpha}| = i\}$, $i \in [\![0, q]\!]$, whose cardinality is equal to the binomial coefficient $\binom{m_s+i-1}{i}$. Thus, the cardinality of the truncation set $\mathcal{A}$, which corresponds to the number of terms in the truncated expansion of PCE denoted $p+1$, is defined by the sum of the cardinalities of the sets $\mathcal{A}_i$:

$$p + 1 = \sum_{i=0}^{q} \frac{(m_s + i - 1)!}{i!(m_s - 1)!} = \frac{(q + m_s)!}{q! m_s!}. \tag{6}$$

However, this truncation can be computationally expensive when the degree of the polynomial interpolation or the number of variables increases. Blatman and Sudret [44, 49] then proposed an adaptive sparse polynomial chaos expansion which is an adaptive modification of the truncation set in order to reduce the value of p.

Considering the truncation associated to Eq. (5), the approximation $\tilde{Y}$ of the system response by PCE reads:

$$\tilde{Y}(\boldsymbol{\xi}) = \sum_{\boldsymbol{\alpha} \in \mathcal{A}} a_{\boldsymbol{\alpha}} \Psi_{\boldsymbol{\alpha}}(\boldsymbol{\xi}), \tag{7}$$

where coefficients $a_{\boldsymbol{\alpha}}$ are to be determined.

2.2 Computation of the coefficients by regression approach

In this study, the regression approach [26, 50] is used to compute the PCE coefficients. This approach is based on a minimization of the quadratic error between the approximation of the system response by PCE and the deterministic system response [27]:

$$\min \left\{ \sum_{j=1}^{n} \left(Y^{(j)} - \tilde{Y}^{(j)} \right)^2 \right\} = \min \left\{ \sum_{j=1}^{n} \left(Y^{(j)} - \sum_{\boldsymbol{\alpha} \in \mathcal{A}} a_{\boldsymbol{\alpha}} \Psi_{\boldsymbol{\alpha}}(\tilde{\boldsymbol{\xi}}^{(j)}) \right)^2 \right\}, \tag{8}$$

on a set of n points, noted $\Xi = \{ \tilde{\boldsymbol{\xi}}^{(j)}, j = 1, \ldots, n\}$, and referred to as the Design of Experiments (DoE). The deterministic system response $Y^{(j)}$ is then evaluated at each isoprobabilistic transformation of the point $\tilde{\boldsymbol{\xi}}^{(j)}$ in order to obtain the vector:

$$\mathbf{Y}_{\text{DoE}} = [Y^{(1)} \ldots Y^{(n)}]^{\intercal}. \tag{9}$$

Additionally, the polynomials of the PCE basis are evaluated at each point of DoE to construct the $\boldsymbol{\Psi}$ matrix:

$$\boldsymbol{\Psi} = \begin{pmatrix} \Psi_{\boldsymbol{\alpha}_0}(\tilde{\boldsymbol{\xi}}^{(1)}) & \Psi_{\boldsymbol{\alpha}_1}(\tilde{\boldsymbol{\xi}}^{(1)}) & \cdots & \Psi_{\boldsymbol{\alpha}_p}(\tilde{\boldsymbol{\xi}}^{(1)}) \\ \vdots & \vdots & \ddots & \vdots \\ \Psi_{\boldsymbol{\alpha}_0}(\tilde{\boldsymbol{\xi}}^{(n)}) & \Psi_{\boldsymbol{\alpha}_1}(\tilde{\boldsymbol{\xi}}^{(n)}) & \cdots & \Psi_{\boldsymbol{\alpha}_p}(\tilde{\boldsymbol{\xi}}^{(n)}) \end{pmatrix}. \tag{10}$$

Finally, the PCE coefficients are determined by:

$$\mathbf{a} = (\boldsymbol{\Psi}^{\intercal} \boldsymbol{\Psi})^{-1} \boldsymbol{\Psi}^{\intercal} \mathbf{Y}_{\text{DoE}}, \tag{11}$$

where $\mathbf{a} = [a_{\boldsymbol{\alpha}_0} \ldots a_{\boldsymbol{\alpha}_p}]^{\intercal}$ and $\boldsymbol{\Psi}^{\intercal} \boldsymbol{\Psi}$ is called the information matrix. For a high number of points n, the information matrix and its inverse may be ill-conditioned [51]. In practice, a singular value decomposition [52] of the information

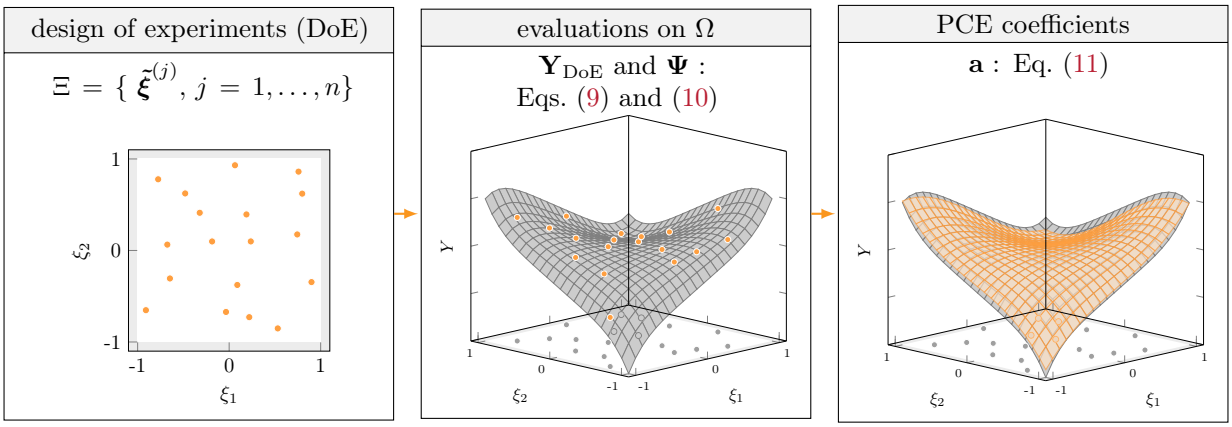

Figure 1. Schematization of the key steps of PCE.

matrix is thus often performed when it is inverted. The key steps for the computation of PCE coefficients are illustrated in Fig. 1.

The selection of the DoE is the cornerstone of the PCE coefficients computation by regression approach. In the literature, there is a wide variety of types of DoE, including the following categories: (1) random points design [53, 54, 55] including random, Latin Hypercube and quasi-random sampling designs, and (2) polynomial root designs [56, 57] constructed with the roots of the univariate polynomial Φ_{q+1}, and (3) alphabetic optimal sampling [58, 59]. There is no unique definition of a DoE and no guideline to determine its appropriate size. The selection of a given type of DoE is oftentimes application specific. Also, while there exists a minimum number of points that should be accounted for in order to guarantee the uniqueness of the PCE coefficients obtained by Eq. (11):

$$n \geq p + 1, \tag{12}$$

the number of points n in a DoE is typically related to computational cost considerations.

2.3 Post-processing of the coefficients

By construction, PCE coefficients $a_{\boldsymbol{\alpha}}$ advantageously allow to compute the mean, the standard deviation and the Sobol indices [51, 60] without computing the approximation of the system response over a large number of runs of the random variables, as is necessary with the Monte Carlo simulations. Indeed, the mean $\tilde{Y}_0$ and the variance $\tilde{D}$ of the system response are straightforwardly computed as follows:

$$\tilde{Y}_0 = \mathrm{E}[\tilde{Y}] = a_{\mathbf{0}}, \tag{13}$$

$$\tilde{D} = \mathrm{Var}[\tilde{Y}] = \sum_{\boldsymbol{\alpha} \in \mathcal{A} \setminus \{\mathbf{0}\}} a_{\boldsymbol{\alpha}}^2. \tag{14}$$

3 Efficient polynomial chaos expansion for permutation invariant and cyclic permutation invariant functions

As mentioned in the introduction, PCE, as presented in section 2, may be ill-suited in the context of some industrial applications such as turbomachinery. This is essentially due to the fact that a very large number of random variables—typically a multiple of the number of blades on the bladed disk—must be considered, thus yielding a compromise to make between accuracy (that often calls for a higher degree of interpolation) and efficacy (which

implies reducing the number of evaluations of the deterministic system). The developments presented in this section aim at taking advantage of the properties of certain types of mathematical systems in order to efficiently apply PCE.

The key steps of the proposed methodology—illustrated in Fig. 2 in the case of two random variables—are:

1. a decomposition of the random space Ω into smaller, well chosen, elementary subspaces $\Omega_{\sigma,l}$,
2. the definition of an elementary DoE, denoted $\Xi_{\sigma,l}$, over one of these subspaces,
3. the evaluations of the deterministic system at each point of $\Xi_{\sigma,l}$,
4. the deployment of the elementary DoE over Ω taking advantage of specific mathematical properties of the investigated systems,
5. the computation of the PCE coefficients.

Reducing the number of required evaluations of the deterministic system to only a few points—significantly less than the theoretical limit given Eq. (12)—belonging to a single subspace $\Omega_{\sigma,l}$ is the key advantage of the proposed methodology. The latter is introduced in a general fashion following a two-step approach. The methodology is first detailed assuming that the investigated system is permutation invariant. Then, it is highlighted that significant gains may also be obtained for cyclic permutation invariant systems, which are of particular interest for a variety of industrial applications.

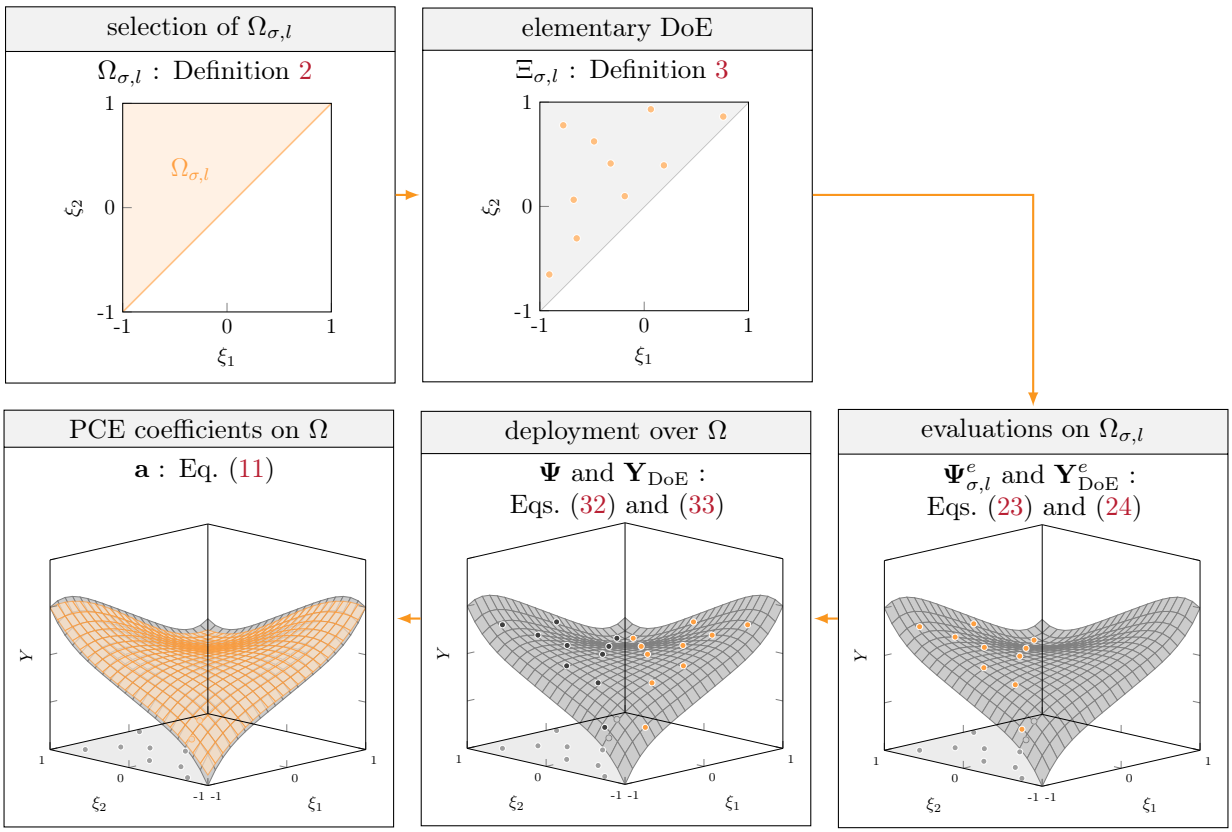

Figure 2. Schematization of the proposed methodology.

For the sake of generality, random variables $\boldsymbol{\xi}_k$, with $k \in [\![1, m_s]\!]$, are here supposed to be d-dimensional vectors:

$$\boldsymbol{\xi}_k = [\xi_{k,1}, \ldots, \xi_{k,d}], \ k \in [\![1, m_s]\!], \tag{15}$$

by extension, the notation $\boldsymbol{\xi} \in \Omega$ thus denotes the set of m_s vectors of random variables:

$$\boldsymbol{\xi} = [\boldsymbol{\xi}_1, \ldots, \boldsymbol{\xi}_{m_s}]^\intercal. \tag{16}$$

The total number of random variables in the system is then equal to $m = m_s d$.

3.1 Improved PCE for permutation invariant functions

3.1.1 Definition of a permutation invariant function

The set of $m_s!$ permutations of integers from 1 to m_s is denoted S_{m_s}. The notation $\boldsymbol{\xi}^{(\sigma)}$ refers to the permutation of the random variables $\boldsymbol{\xi}$ for $\sigma \in S_{m_s}$:

$$\boldsymbol{\xi}^{(\sigma)} = [\boldsymbol{\xi}_{\sigma(1)}, \dots, \boldsymbol{\xi}_{\sigma(m_s)}]^\intercal, \tag{17}$$

where :

$$\boldsymbol{\xi}_{\sigma(k)} = [\xi_{\sigma(k),1}, \dots, \xi_{\sigma(k),d}], \forall k \in [\![1, m_s]\!]. \tag{18}$$

In the remainder, the response Y of the considered system is assumed to be permutation invariant.

Definition 1. *A function f defined on $\mathbb{R}^m$ is said to be permutation invariant if and only if :*

$$\forall \boldsymbol{\xi} \in \mathbb{R}^m, \forall \sigma \in S_{m_s}, \quad f(\boldsymbol{\xi}) = f(\boldsymbol{\xi}^{(\sigma)}). \tag{19}$$

3.1.2 Decomposition of the random space Ω

Definition 2. *Let σ be a permutation of S_{m_s} and $l \in [\![1, d]\!]$ be an index. The subspace $\Omega_{\sigma,l}$ of the random space Ω is defined as:*

$$\Omega_{\sigma,l} = \{\boldsymbol{\xi} \in \Omega \,|\, \forall k \in [\![1, m_s - 1]\!],\ \xi_{\sigma(k),l} \leq \xi_{\sigma(k+1),l}\}. \tag{20}$$

The subspace $\Omega_{\sigma,l}$ thus defined is related to an order relation in $\mathbb{R}$ between the l-th coordinates of each variable ξ_k, with $k \in [\![1, m_s]\!]$. The demonstrations of the following theorems are respectively given in A, B and C.

Theorem 1. *Let σ be a permutation of S_{m_s} and $l \in [\![1, d]\!]$ be an index. The subspace $\Omega_{\sigma,l}$ verifies the following properties :*
(i) $\Omega_{\sigma,l}$ is compact,
(ii) $\Omega_{\sigma,l}$ is convex,
(iii) the boundary of $\Omega_{\sigma,l}$ is a null set.

Theorem 2. *Let σ_1 and σ_2 be two permutations of S_{m_s} and $l \in [\![1, d]\!]$ be an index. The boundary of $\Omega_{\sigma_1,l} \bigcap \Omega_{\sigma_2,l}$ is a null set.*

Theorem 3. *Let $l \in [\![1, d]\!]$ be an index. The boundary of $\bigcup_{\sigma \in S_{m_s}} \Omega_{\sigma,l}$ is a null set.*

Remark 1. *For any index l, it is may be proven that:*

$$\bigcup_{\sigma \in S_{m_s}} \Omega_{\sigma,l} = \Omega. \tag{21}$$

Based on definition 2, the random space Ω is here decomposed into subspaces $\Omega_{\sigma,l}$. It should be noted that this decomposition is not unique as it arbitrarily depends on the chosen index l. For a given l, theorems 1, 2 and 3, combined with remark 1, highlight that the proposed decomposition is optimal since the intersection of any two subspaces is a null set. For this reason, subspaces $\Omega_{\sigma,l}$ are referred to as *elementary subspaces* in the remainder. For illustration purposes, an elementary subspace is depicted in the case of $m_s = 2$ and $m_s = 3$ in Fig. 3.

3.1.3 Elementary design of experiments

Definition 3. *Let σ be a permutation of S_{m_s} and $l \in [\![1, d]\!]$ be an index so that $\Omega_{\sigma,l}$ denotes an elementary subspace of Ω. The elementary design of experiments, noted $\Xi_{\sigma,l}$, is defined as a set of n_e distinct points in $\Omega_{\sigma,l}$:*

$$\Xi_{\sigma,l} = \{\boldsymbol{\xi}^{(j)} \in \Omega_{\sigma,l},\ j = 1, \dots, n_e\}. \tag{22}$$

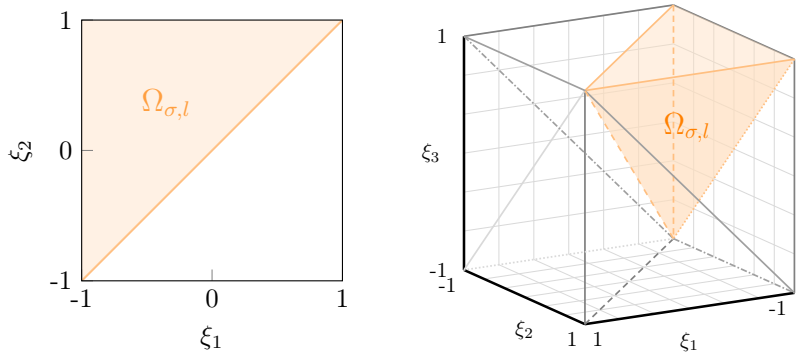

(a) (b)

Figure 3. Visual representation of an elementary subspace ( ) for different values of m_s. (a) $m_s = 2$; (b) $m_s = 3$.

For a given elementary subspace $\Omega_{\sigma,l}$, the definition of a specific DoE on $\Omega_{\sigma,l}$—following any of the listed methodologies in section 2—denoted $\Xi_{\sigma,l}$ and referred to as *elementary DoE*, see definition 3, leads to the construction of an elementay matrix $\mathbf{\Psi}^e_{\sigma,l}$ analogous to the one defined in Eq. (10):

$$\mathbf{\Psi}^e_{\sigma,l} = \begin{pmatrix} \Psi_{\boldsymbol{\alpha}_0}(\boldsymbol{\xi}^{(1)}) & \Psi_{\boldsymbol{\alpha}_1}(\boldsymbol{\xi}^{(1)}) & \cdots & \Psi_{\boldsymbol{\alpha}_p}(\boldsymbol{\xi}^{(1)}) \\ \vdots & \vdots & \ddots & \vdots \\ \Psi_{\boldsymbol{\alpha}_0}(\boldsymbol{\xi}^{(n_e)}) & \Psi_{\boldsymbol{\alpha}_1}(\boldsymbol{\xi}^{(n_e)}) & \cdots & \Psi_{\boldsymbol{\alpha}_p}(\boldsymbol{\xi}^{(n_e)}) \end{pmatrix}, \ \boldsymbol{\xi}^{(j)} \in \Xi_{\sigma,l}, \ j = 1, \dots, n_e, \tag{23}$$

and the evaluations of the system response over $\Xi_{\sigma,l}$, noted $\mathbf{Y}^e_{\text{DoE}}$, defined as:

$$\mathbf{Y}^e_{\text{DoE}} = [Y^{(1)} \dots Y^{(n_e)}]^\intercal. \tag{24}$$

3.1.4 Deployment over the random space Ω

For the sake of readability, the demonstrations of theorems 4 and 5 are respectively given in D and E.

Definition 4. *Let σ be a permutation of S_{m_s} and $l \in [\![1, d]\!]$ be an index so that $\Xi_{\sigma,l}$ denotes an elementary DoE of the elementary subspace $\Omega_{\sigma,l}$. The DoE Ξ is defined as the union of the permutations of the n_e points of $\Xi_{\sigma,l}$:*

$$\Xi = \left\{ \bigcup_{\hat{\sigma} \in S_{m_s}} \{ \boldsymbol{\xi}^{(\hat{\sigma})} \}, \forall \boldsymbol{\xi} \in \Xi_{\sigma,l} \right\}. \tag{25}$$

Theorem 4. *For any permutation $\sigma \in S_{m_s}$, for any index $l \in [\![1, d]\!]$, for any point $\boldsymbol{\xi} \in \Omega$, it is possible to build a DoE Ξ from an elementary DoE $\Xi_{\sigma,l}$ such as $\boldsymbol{\xi} \in \Xi$:*

$$\forall \sigma \in S_{m_s}, \forall l \in [\![1, d]\!], \forall \boldsymbol{\xi} \in \Omega, \exists \Xi_{\sigma,l} \subset \Omega_{\sigma,l}, \boldsymbol{\xi} \in \Xi. \tag{26}$$

Theorem 5. *Let σ be a permutation of S_{m_s} and $l \in [\![1, d]\!]$ be an index so that Ξ denotes the DoE deployed from $\Xi_{\sigma,l}$. The cardinal n of Ξ satisfies:*

$$n \leq m_s! n_e, \tag{27}$$

with equality if the points of $\Xi_{\sigma,l}$ are selected in the interior of $\Omega_{\sigma,l}$. In which case, all points of Ξ are distinct.

Remark 2. *Any point of $\Xi_{\sigma,l}$ that belongs to the intersection of $\Omega_{\sigma,l}$ with another elementary subspace will be duplicated in Ξ, this leads to redundant evaluations for the computation of the PCE. In order to avoid such redundancy, it is sufficient, from Theorem 5, to select points of $\Xi_{\sigma,l}$ in the interior of $\Omega_{\sigma,l}$.*

Assuming an elementary DoE $\Xi_{\sigma,l}$ is defined in the elementary subspace $\Omega_{\sigma,l}$, definition 4 yields the DoE Ξ that spans over the full random space Ω. Theorem 4 highlights that, for any given point $\boldsymbol{\xi} \in \Omega$, there is a way to build $\Xi_{\sigma,l}$ so that $\boldsymbol{\xi}$ belongs to Ξ. This is important as it underlines that the proposed methodology does not imply any restriction on the definition of Ξ which may thus include any point of the random space. In order to maximize the efficacy of the methodology and to ensure that all points of Ξ are distinct, theorem 5 and remark 2 yields the recommendation that all points of $\Xi_{\sigma,l}$ belong to the interior of $\Omega_{\sigma,l}$.

3.1.5 PCE coefficients

The proof of the following theorem may be found in F.

Theorem 6. *Let σ be a permutation of S_{m_s} and $l \in [\![1,d]\!]$ be an index so that Ξ denotes the DoE defined from $\Xi_{\sigma,l}$.*

$$\forall \boldsymbol{\xi} \in \Xi, \exists \hat{\sigma} \in S_{m_s},\ \boldsymbol{\xi}^{(\hat{\sigma})} \in \Xi_{\sigma,l} \text{ and } \forall \boldsymbol{\alpha} \in \mathcal{A},\ \Psi_{\boldsymbol{\alpha}}(\boldsymbol{\xi}) = \Psi_{\boldsymbol{\alpha}^{(\hat{\sigma})}}(\boldsymbol{\xi}^{(\hat{\sigma})}), \tag{28}$$

where $\boldsymbol{\alpha}^{(\hat{\sigma})} = [\boldsymbol{\alpha}_1^{(\hat{\sigma})}, \dots, \boldsymbol{\alpha}_{m_s}^{(\hat{\sigma})}]$ refers to the permutation of the multi-index $\boldsymbol{\alpha}$ for $\hat{\sigma}$:

$$\alpha_{k,h}^{(\hat{\sigma})} = \alpha_{\hat{\sigma}(k),h}, \forall k \in [\![1, m_s]\!], \forall h \in [\![1,d]\!]. \tag{29}$$

Computation of the matrix $\boldsymbol{\Psi}$. For any permutation $\hat{\sigma} \in S_{m_s}$ theorem 6 underlines that there exists an explicit relation between $\boldsymbol{\Psi}^e_{\sigma,l}$ and $\boldsymbol{\Psi}^e_{\hat{\sigma},l}$:

$$\boldsymbol{\Psi}^e_{\hat{\sigma},l} = \boldsymbol{\Psi}^e_{\sigma,l} \mathbf{P}_{\hat{\sigma}}, \tag{30}$$

where $\mathbf{P}_{\hat{\sigma}}$ is the permutation matrix:

$$\forall i \in [\![0,p]\!], \forall \hat{\imath} \in [\![0,p]\!], \quad (\mathbf{P}_{\hat{\sigma}})_{i\hat{\imath}} = \begin{cases} 1 & \text{if} \quad \alpha^{(i)}_{k,h} = \alpha^{(\hat{\imath})}_{\hat{\sigma}(k),h}, \forall k \in [\![1,m_s]\!], \forall h \in [\![1,d]\!], \\ 0 & \text{otherwise.} \end{cases} \tag{31}$$

Therefore, the matrix $\boldsymbol{\Psi}$ defined in Eq. (10) may be obtained from:

$$\boldsymbol{\Psi} = \|_{\hat{\sigma} \in S_{m_s}} \boldsymbol{\Psi}^e_{\hat{\sigma},l} = \|_{\hat{\sigma} \in S_{m_s}} \boldsymbol{\Psi}^e_{\sigma,l} \mathbf{P}_{\hat{\sigma}}, \tag{32}$$

where $\|$ is the matrix concatenation symbol. Equation (32) underlines that $\boldsymbol{\Psi}$ solely depends on $\boldsymbol{\Psi}^e_{\sigma,l}$ so that polynomial evaluations are only required over the elementary DoE $\Xi_{\sigma,l}$.

Computation of the vector $\mathbf{Y}_{\mathbf{DoE}}$. Based on the definition of Ξ, see definition 4, and the fact that the considered system is permutation invariant, the evaluations of the system response over Ξ are actually a repetition ($m_s!$ times) of the elementary evaluation vector defined in Eq. (24):

$$\mathbf{Y}_{\mathrm{DoE}} = \underbrace{[\mathbf{Y}^e_{\mathrm{DoE}} \mathbf{Y}^e_{\mathrm{DoE}} \dots \mathbf{Y}^e_{\mathrm{DoE}}]^\intercal}_{m_s! \text{ times}}. \tag{33}$$

Equations (32) and (33) yield the computation of the information matrix and the polynomial coefficients in an identical fashion to what is done for the standard PCE approach with Eq. (11). Consequently, the proposed approach yields identical PCE coefficients but requires $m_s!$ times less evaluations of the deterministic system. In the following, the proposed methodology is referred to as Polynomial Chaos Expansion for Permutation Invariant systems (PI-PCE).

3.1.6 Application: analytical test case

PI-PCE is here applied to a simple permutation invariant analytical system Y defined as follows:

$$Y(X_1, X_2) = X_1^5 + X_2^5 - 2X_1X_2. \tag{34}$$

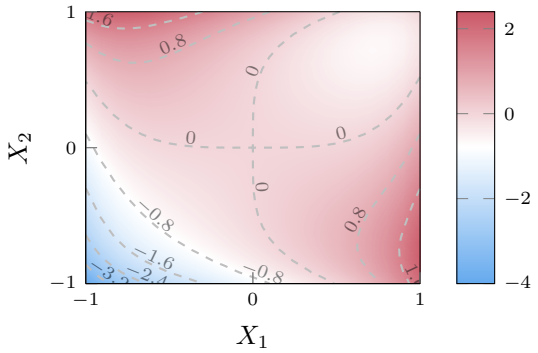

Figure 4. Analytical system $Y(X_1, X_2)$.

For this test case, two scalar random variables (X_1, X_2) are considered ($m_s = 2$, $d = 1$). These random variables are uniformly distributed over $[-1, 1]$. The permutation invariance of Y is obvious as $Y(X_1, X_2) = Y(X_2, X_1)$, $\forall X_1, X_2 \in [-1, 1]$. The exact value of Y over the random space may be computed at no significant computational cost and is depicted in Fig. 4 that will serve as a reference point in this section.

All computations are carried out with a degree $q = 3$ thus yielding $p + 1 = 10$ terms in the PCE basis, composed of Legendre polynomials in agreement with the Askey scheme. PI-PCE is applied as follows:

1. the elementary subspace $\Omega_{\sigma,l}$ is defined as:

$$\Omega_{\sigma,l} = \{(\xi_1, \xi_2) \in \Omega \,|\, \xi_1 < \xi_2\}, \tag{35}$$

2. $n_e = 10$ points are randomly selected in the interior of $\Omega_{\sigma,l}$ to define the elementary DoE $\Xi_{\sigma,l}$,
3. the deployed DoE Ξ thus contains 20 points and is used for computation of the standard PCE.

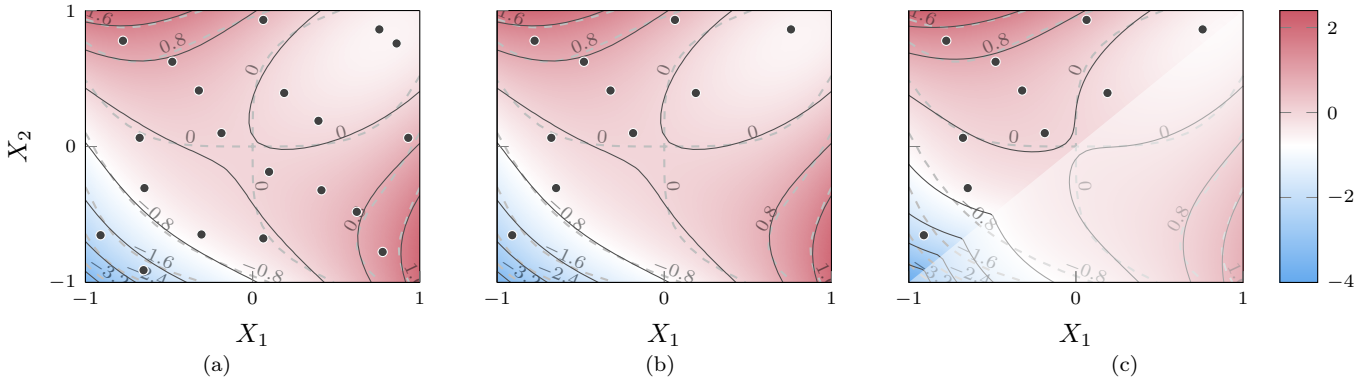

Figure 5. System's response computed with the different methodologies, required system evaluation points (•). (a) standard PCE; (b) PI-PCE; (c) ME-PCE.

Results obtained with the standard PCE and PI-PCE are respectively depicted in Figs. 5(a) and 5(b). Additionally, results obtained with the Multi-Element PCE (ME-PCE) [42] are plotted in Fig. 5(c). While PI-PCE requires half of the evaluations necessary for standard PCE, results obtained with both methods are numerically identical, as evidenced in Fig. 6(a). In comparison, ME-PCE yields non-negligible errors, including a non-smooth connection along the line $X_1 = X_2$.

3.2 Improved PCE for cyclic permutation invariant functions

The principle of PI-PCE is here extended to cyclic permutation invariant mathematical systems.

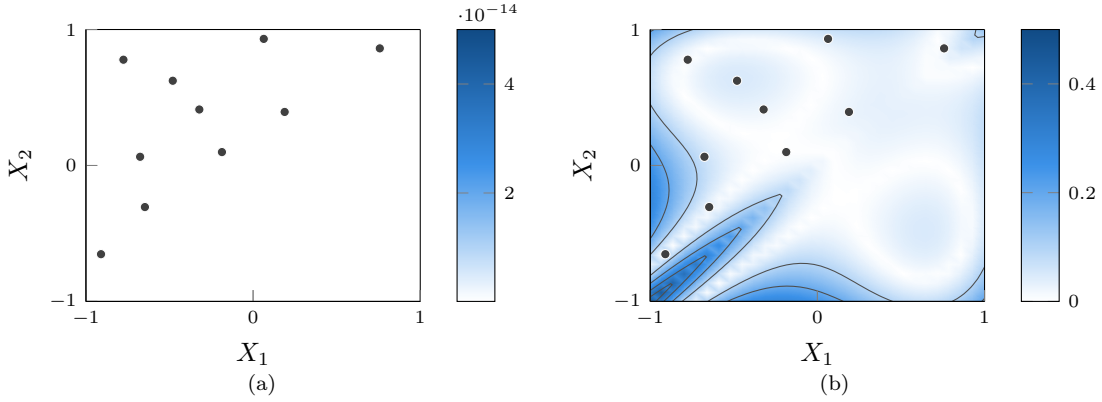

Figure 6. Absolute errors with respect to standard PCE. (a) PI-PCE; (b) ME-PCE.

3.2.1 Definition of a cyclic permutation invariant function

The set of m_s cyclic permutations of integers ranging from 1 to m_s is denoted C_{m_s}:

$$C_{m_s} = \{\ (\overline{k}, \overline{k+1}, \ldots, \overline{k+m_s-1}) \mid \forall k \in [\![1, m_s]\!]\}, \tag{36}$$

where $\overline{k} = k \pmod{m_s}$, with $k \in \{1, 2, \ldots, m_s\}$. In the remainder, the response Y of the considered system is assumed to be cyclic permutation invariant.

Definition 5. *A function f defined on $\mathbb{R}^m$ is said to be cyclic permutation invariant if and only if:*

$$\forall \boldsymbol{\xi} \in \mathbb{R}^m, \forall \sigma \in C_{m_s}, \quad f(\boldsymbol{\xi}) = f(\boldsymbol{\xi}^{(\sigma)}). \tag{37}$$

3.2.2 Mathematical framework

Definition 6. *Let $\sigma \in C_{m_s}$ be a cyclic permutation. Let $l \in [\![1, d]\!]$ be an index. The subspace $\Omega_{\sigma,l}$ of the random space Ω is defined as:*

$$\Omega_{\sigma,l} = \{\boldsymbol{\xi} \in \Omega \,|\, \forall k \in [\![2, m_s]\!],\ \xi_{\sigma(1),l} \leq \xi_{\sigma(k),l}\}. \tag{38}$$

Definition 7. *Let σ be a permutation of C_{m_s} and $l \in [\![1, d]\!]$ be an index so that $\Omega_{\sigma,l}$ denotes an elementary subspace of Ω. The elementary design of experiments, noted $\Xi_{\sigma,l}$, is defined as a set of n_e distinct points in $\Omega_{\sigma,l}$:*

$$\Xi_{\sigma,l} = \{\boldsymbol{\xi}^{(j)} \in \Omega_{\sigma,l},\ j = 1, \ldots, n_e\}. \tag{39}$$

Theorem 7. *Let σ be a permutation of C_{m_s} and $l \in [\![1, d]\!]$ be an index so that Ξ denotes the DoE deployed from $\Xi_{\sigma,l}$. The cardinal n of Ξ satisfies:*

$$n \leq m_s n_e, \tag{40}$$

with equality if the points of $\Xi_{\sigma,l}$ are selected from the interior of $\Omega_{\sigma,l}$. In which case, all points of Ξ are distinct.

The proof of theorem 7 is similar to the one of theorem 5, that may be found in E, substituting S_{m_s} for C_{m_s}.

Based on definition 6, the random space is here decomposed into subspaces $\Omega_{\sigma,l}$, related to an order relation in $\mathbb{R}$ between the l-th coordinates of the variable $\boldsymbol{\xi}_{\sigma(1)}$ and the other variables $\boldsymbol{\xi}_{\sigma(k)}$, with $k \in [\![2, m_s]\!]$. Because C_{m_s} is a subset of S_{m_s}, theorems 1, 2 and 3, as well as remark 1, hold. As a consequence, similarly to what was shown in section 3.1.2, the decomposition of the random space Ω into the subspaces $\Omega_{\sigma,l}$ is optimal in the sense that the intersection of any two subspaces is a null set. Subspaces $\Omega_{\sigma,l}$ are thus referred to as *elementary subspaces* in the following. For illustration purposes, an elementary subspace is depicted for $m_s = 3$ random variables in Fig. 7.

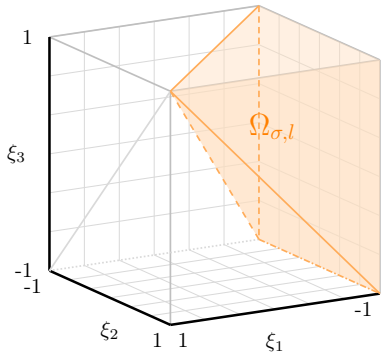

Figure 7. Visual representation of an elementary subspace ( ) for $m_s = 3$.

An elementary DoE $\Xi_{\sigma,l}$ is defined over the elementary subspace $\Omega_{\sigma,l}$ according to definition 7. Definition 4 and theorem 4 hold true for any cyclic permutation. From that point, the application of theorem 7 ensures that the DoE Ξ spans over the full random space Ω and that, assuming all points of $\Xi_{\sigma,l}$ are selected in the interior of $\Omega_{\sigma,l}$, all points of Ξ will be distinct. Theorem 6 remains valid and the proposed methodology then enfolds similarly to what is presented in section 3.1.5.

One may note that, when considering cyclic permutation invariant systems, there are m_s elementary subspaces (in comparison to the $m_s!$ subspaces identified in section 3.1.2), which implies that the proposed methodology yields a reduction of the number of required evaluations of the deterministic system by a factor m_s. In the following, the proposed methodology is referred to as Polynomial Chaos Expansion for Cyclic permutation Invariant systems (CI-PCE). One may note that the theoretical minimum number of evaluations n required for PCE given in Eq. (12) is significantly reduced. Indeed, only n_e evaluations are required for CI-PCE, with:

$$n_e \geq \left\lfloor \frac{p+1}{m_s} \right\rfloor + 1. \tag{41}$$

3.2.3 Application: analytical test case

CI-PCE is here applied to a cyclic permutation invariant analytical system Y defined as follows:

$$Y(\mathbf{X}_1, \mathbf{X}_2, \mathbf{X}_3) = \mathrm{Tr}(\mathbf{V}(\mathbf{X}_1)\mathbf{V}(\mathbf{X}_2)\mathbf{V}(\mathbf{X}_3)), \tag{42}$$

where the random variables $\mathbf{X}_k$, with $k \in \{1, 2, 3\}$, are here considered to be 2-dimensional vectors ($m_s = 3$, $d = 2$), and each matrix $\mathbf{V}(\mathbf{X}_k)$ is defined by:

$$\mathbf{V}(\mathbf{X}_k) = \begin{pmatrix} 1 & X_{k,1} & X_{k,1}^2 \\ 1 & X_{k,2} & X_{k,2}^2 \\ 1 & X_{k,1}X_{k,2} & X_{k,1}^2 X_{k,2}^2 \end{pmatrix}, \ k \in \{1, 2, 3\}. \tag{43}$$

For this test case, the random variables $(X_{k,1}, X_{k,2})$, with $k \in \{1, 2, 3\}$, are uniformly distributed respectively over $[0.5, 1.5]$ and $[0, 1]$. The function Y is indeed cyclic permutation invariant, thanks to the mathematical property of the trace function, it may be easily shown that: $Y(\mathbf{X}_1, \mathbf{X}_2, \mathbf{X}_3) = Y(\mathbf{X}_3, \mathbf{X}_1, \mathbf{X}_2) = Y(\mathbf{X}_2, \mathbf{X}_3, \mathbf{X}_1)$, $\forall \mathbf{X}_1, \mathbf{X}_2, \mathbf{X}_3 \in \mathbb{R}^2$.

The reference value of Y is here computed by Monte Carlo simulations using a large random sampling ($N = 50\,000$). PCE and CI-PCE computations are carried out with a degree $q = 3$ thus yielding $p + 1 = 84$ terms in the PCE basis composed of Legendre polynomials in accordance with the Askey scheme. Two PCE are computed as follows:

1. standard PCE so that the DoE is composed of the minimum number of required evaluations: $p + 1$ random points of Ω,
2. CI-PCE with an elementary DoE comprising the same number of points: $p + 1$.

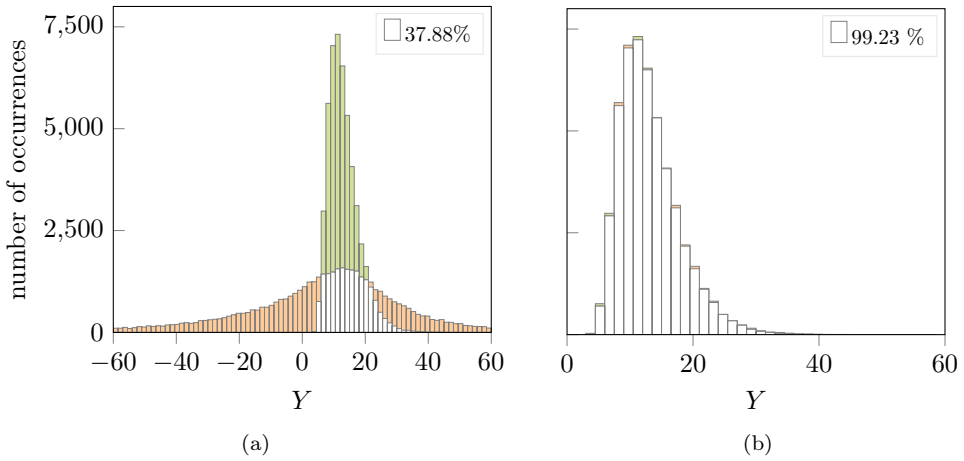

Figure 8. PDF of the system response computed by MCS (■) and: (a) PCE (■); (b) CI-PCE (■).

Probability Density Functions (PDF) obtained with the PCE and CI-PCE are respectively depicted in Figs. 8(a) and 8(b). These results (■) are superimposed with the MCS results (■). For each bin of the histogram, the white area (□) corresponds to the minimum value of the two compared PDF. In the following, the ratio of the intersection thus represents the percentage of white area with respect to the total area of MCS results. For the sake of readability, this quantity is provided on the top right corner of each figure. While CI-PCE is built with the same number of points as the standard PCE, it is patent that the obtained results are significantly improved with no additional computational cost.

4 Industrial application: mistuned bladed disk analysis

This section is dedicated to the analysis of the influence of mistuning on bladed disks [6]. The vibration behavior of a mistuned bladed disk has been extensively described in the literature [10], it notably features: (1) a possible localization of the vibration energy on a few blades, (2) the split of eigenfrequencies and (3) a potentially significant increase in forced response amplitudes. The latter, known as amplitude magnification [4], is defined as the ratio between the maximum amplitude predicted for mistuned configurations and the amplitude predicted for the tuned bladed disk. Amplitudes are computed based on the steady state response of the bladed disk model under a traveling wave excitation [4, 12]. While recent investigations have underlined that amplitude magnification may be difficult to predict with PCE [27], it is here shown that under certain conditions, it is possible to benefit from the computational efficiency of CI-PCE to obtain more accurate results at a low computational cost, even for large industrial finite element models.

The first subsection highlights that when considering the computation of a mistuned bladed disk's eigenfrequencies or amplitude magnification, the underlying mathematical system is cyclic permutation invariant so that CI-PCE may be applied. CI-PCE is then applied to two bladed disk models: (1) a simplified model previously analyzed in the literature [46], and (2) an industrial compressor stage.

4.1 Cyclic permutation invariance of mistuned bladed disk models

As is often the case in the literature, mistuning is accounted for in this study through a variation of certain mechanical properties from a blade to another. More precisely, assuming a perfectly cyclically symmetric model of a bladed disk with m_s blades, a single ($d = 1$) random variable—that may be an equivalent stiffness k_i or the Young's modulus E_i of the i-th blade—is here considered. The variation of these quantities is denoted δ_i, and the set of all these variations $[\delta_1, \ldots, \delta_{m_s}]$ defines the mistuning pattern [61].

In the following, the influence of mistuning is solely assessed through the variation of a bladed disk's eigenfrequencies and amplitude magnification. For illustration purposes, a random mistuning pattern $[\delta_1, \ldots, \delta_{21}]$ of a

21-blade bladed disk is depicted alongside each blade's vibration amplitude for a given external forcing in Fig. 9(a). The cyclic permutation of this mistuning pattern $[\delta_{19}, \delta_{20}, \delta_{21}, \delta_1, \ldots, \delta_{18}]$ yields a cyclic permutation of predicted blade's vibration amplitudes, see Fig. 9(b). However, because the amplitude magnification is defined relatively to the maximum vibration amplitude over the whole bladed disk, it is unaffected by the mistuning pattern cyclic permutation. For this reason, the mathematical function that computes the amplitude magnification of a bladed disk is cyclic permutation invariant when considering the proposed mistuning modeling. Similarly, the mathematical function yielding the computation of a bladed disk's eigenfrequencies is also cyclic permutation invariant and CI-PCE may be applied in both cases.

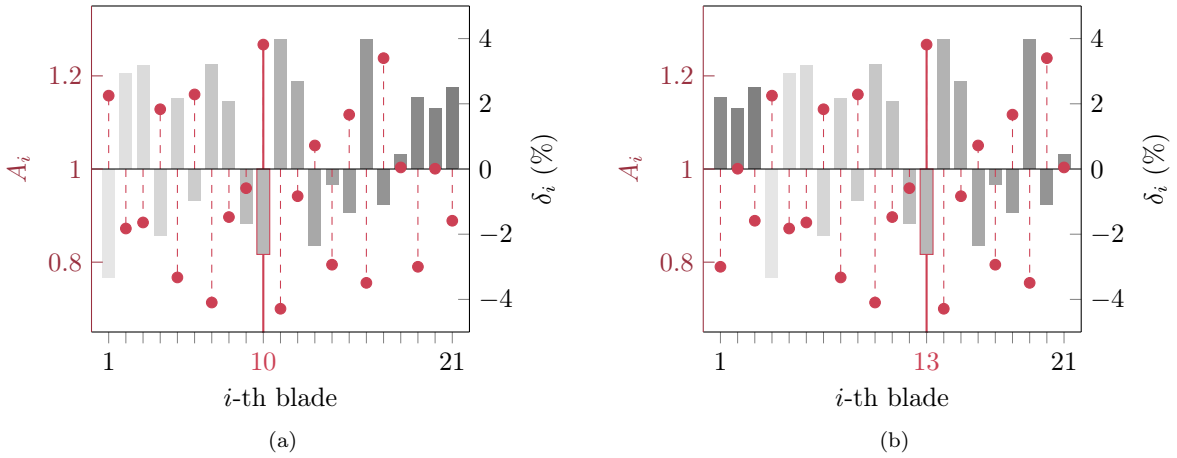

Figure 9. Amplitude magnifications (●) of a mistuned 21-blade bladed disk for: (a) initial mistuning pattern (■); (b) cyclic permutation of the initial mistuning pattern.

4.2 Simple model of a bladed disk

In this section, CI-PCE is applied to a simple lumped mass model of bladed disk which was previously investigated in the literature [46, 19]. The two quantities of interest are the amplitude magnification of the first blade, denoted A_1, and the amplitude magnification of the bladed disk, denoted A and defined by:

$$A = \max_{i \in [\![1, m_s]\!]} A_i, \tag{44}$$

where m_s is the number of blades in the system.

As explained in the previous section, the function $A = f(\delta_1, \ldots, \delta_{m_s})$ is cyclic permutation invariant so that CI-PCE may be directly applied. However, the function $[A_1, \ldots, A_{m_s}] = g(\delta_1, \ldots, \delta_{m_s})$ is not cyclic permutation invariant. In order to apply CI-PCE for the approximation of g, one must account for the fact that a cyclic permutation of the inputs yields the same cyclic permutation of the outputs, as illustrated in Fig. 9. As a consequence, the application of CI-PCE for g simply requires that the evaluation vector in Eq. (33) be modified as follows:

$$\mathbf{Y}_{\mathrm{DoE}} = \|_{\hat{\sigma} \in C_{m_s}} \mathbf{Y}^{e,(\hat{\sigma})}_{\mathrm{DoE}}, \tag{45}$$

where $\mathbf{Y}^{e,(\hat{\sigma})}_{\mathrm{DoE}}$ refers to the evaluations of the system response $[A_1, \ldots, A_{m_s}]$ at the permutation $\hat{\sigma}$ of the n_e points $\boldsymbol{\xi}^{(j)}$ of the elementary DoE:

$$\left(\mathbf{Y}^{e,(\hat{\sigma})}_{\mathrm{DoE}}\right)_j = [Y^{(j)}_{\hat{\sigma}(1)}, \ldots, Y^{(j)}_{\hat{\sigma}(m_s)}] = [A^{(j)}_{\hat{\sigma}(1)}, \ldots, A^{(j)}_{\hat{\sigma}(m_s)}],\ j \in [\![1, n_e]\!]. \tag{46}$$

This modification does not imply any significant increase in terms of computational cost of CI-PCE.

4.2.1 Model parameters and mistuning modeling

As depicted in Fig. 10, the lumped mass model consists of a chain of m_s single degree-of-freedom oscillators. The parameters of the model, identical to those considered in previous publications [46], are detailed in Tab. 1. In the following, mistuning is represented by a variation of the stiffness k_i of each blade defined as:

$$k_i = k_b(1 + \delta_i),\ i \in [\![1, m_s]\!], \tag{47}$$

where k_b is the nominal blade stiffness. It is assumed that the stiffness of each blade follows a normal distribution whose mean and standard deviation are respectively $k_b = 430\,000\,\mathrm{N\,m^{-1}}$ and $\sigma_b = 10\,000\,\mathrm{N\,m^{-1}}$.

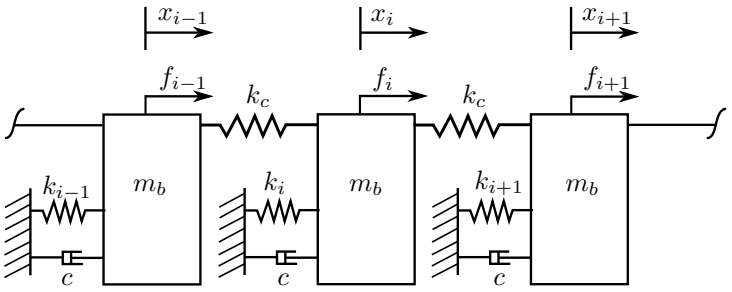

Figure 10. Schematic representation of the simple lumped mass model. Adapted from [46].

variable	description	value	unit
m_s	number of blades	10	-
k_b	nominal blade stiffness	430 000	$\mathrm{N\,m^{-1}}$
m_b	blade mass	0.0114	kg
k_c	coupling stiffness	45 430	$\mathrm{N\,m^{-1}}$
c	damping coefficient	1.43	$\mathrm{N\,s\,m^{-1}}$
f_0	excitation force	1	N
r	engine order	3	-

Table 1. Mechanical parameters of the simple lumped mass model.

In order to validate the implementation of the model and the way mistuning is accounted for, amplitude magnifications A_1 and A obtained with MCS considering $N = 10\,000$ random samples are confronted to previously published results [46]. PDF of these two quantities are depicted in Figs. 11(a) and 11(b). Previously published results for these same two quantities are pictured in Figs. 11(c) and 11(d). Overall, there is an excellent agreement between the obtained results and the published results. The very minor differences that may be seen are assumed to be related to a non-identical random sampling procedure.

4.2.2 PCE approximation

PCE is here used to approximate the values of A_1 and A. PCE is carried out considering a degree $q = 3$—yielding $p + 1 = 286$ terms in the PCE basis—and a DoE comprising $n = 2(p + 1) = 572$ random points. The PCE approximation of the system response over $N = 10\,000$ random samples is thereafter compared to Monte Carlo simulations. The same color code as the one used in Fig. 8 is employed in this section: PCE results (■) are superimposed with the MCS results (■) and the ratio of their intersection (□) is provided as a percentage on the top right corner of each figure.

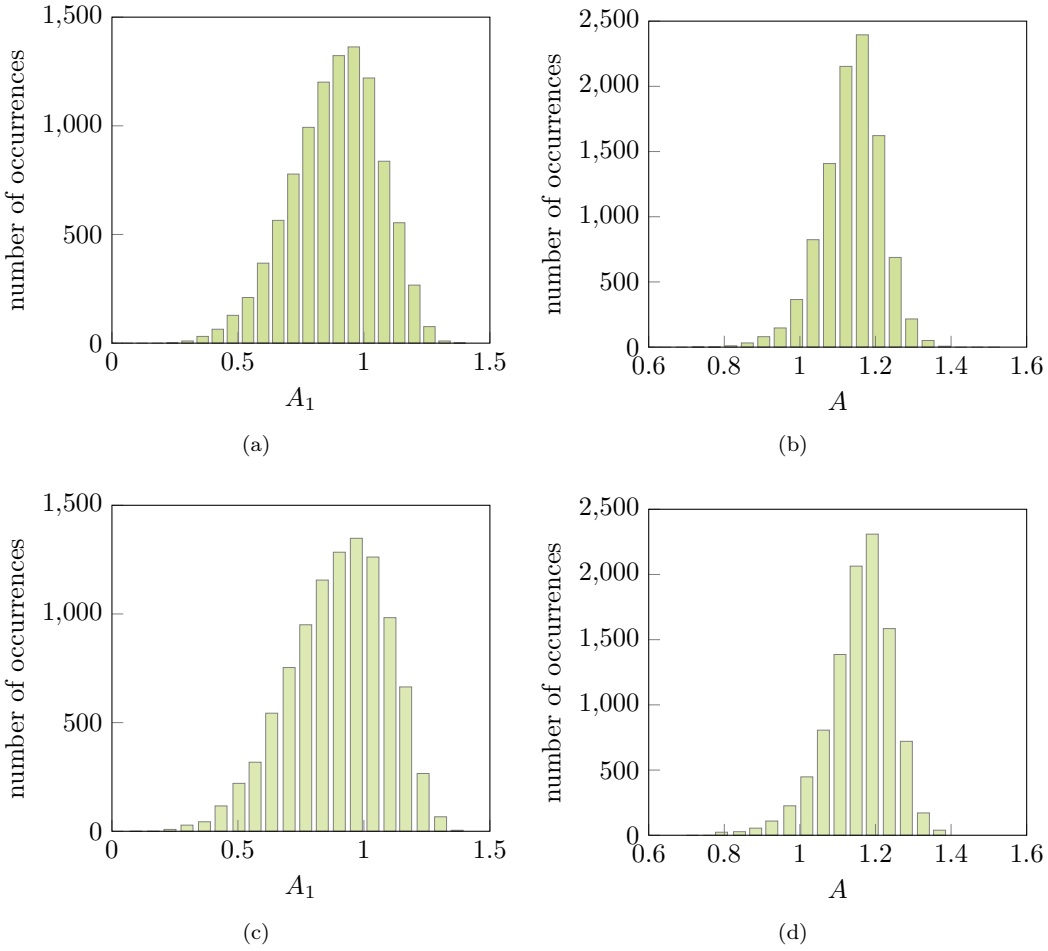

Figure 11. Monte Carlo simulations results for: (a) PDF of A_1; (b) PDF of A; (c) reference PDF of A_1 [46]; (d) reference PDF of A [46].

The PDF of A_1 and A obtained by PCE are respectively depicted in Figs. 12(a) and 12(b). PCE provides a better approximation of A_1 (intersection ratio of 98.36%) than A (intersection ratio of 87.73%). This observation is consistent with the fact that the function $A = f(\delta_1, \ldots, \delta_{m_s})$ is non-smooth due to the max function in Eq. (44). It is well-known that PCE may perform poorly for such functions [62]. Therefore, in order to improve the quality of the PCE results for A, it is now computed indirectly: all the A_i values are first obtained with one PCE and A is computed *a posteriori* by means of Eq. (44). Corresponding PCE results for A are depicted in Fig. 13 with a superimposition on a scatter plot (Fig. 13(a)) of samples obtained by the direct PCE computation of A (+) and those obtained with the indirect PCE computation of A (+), alongside the PDF with the indirect PCE computation, see Fig. 13(b).

The improvement of the results is confirmed by the fact that, the Pearson correlation coefficients are 0.6247 for the direct PCE computation and 0.9329 for the indirect PCE computation of A. It is also noticeable that the intersection ratio significantly increases between Fig. 12(b) and Fig. 13(b).

In conclusion, these results confirm that the chosen PCE parameters $q = 3$ and $n = 572$ yield a very good approximation of both A_1 and A assuming the latter is computed indirectly, which will always be the case in the following.

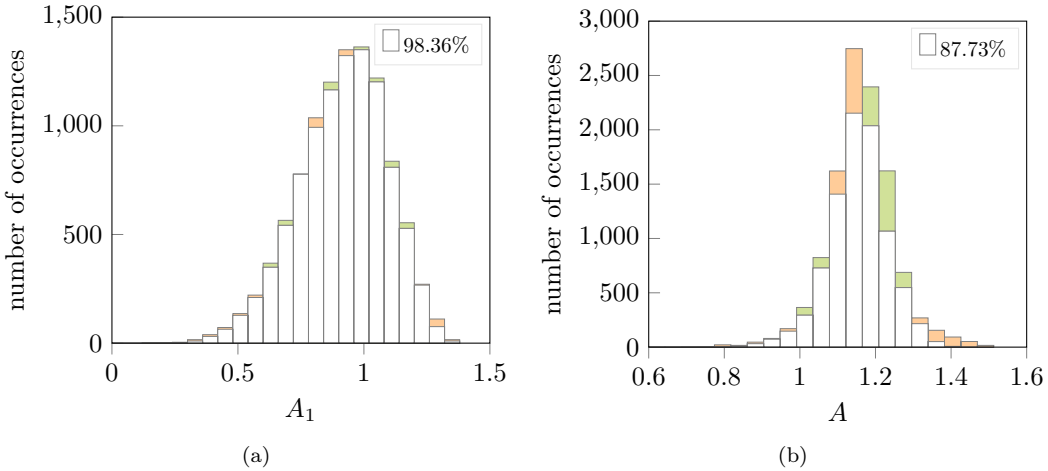

Figure 12. PDF of A and A_1 by MCS (■) and PCE (■) ($q = 3$ and $n = 572$). (a) amplitude magnification of the first blade; (b) amplitude magnification of the bladed disk.

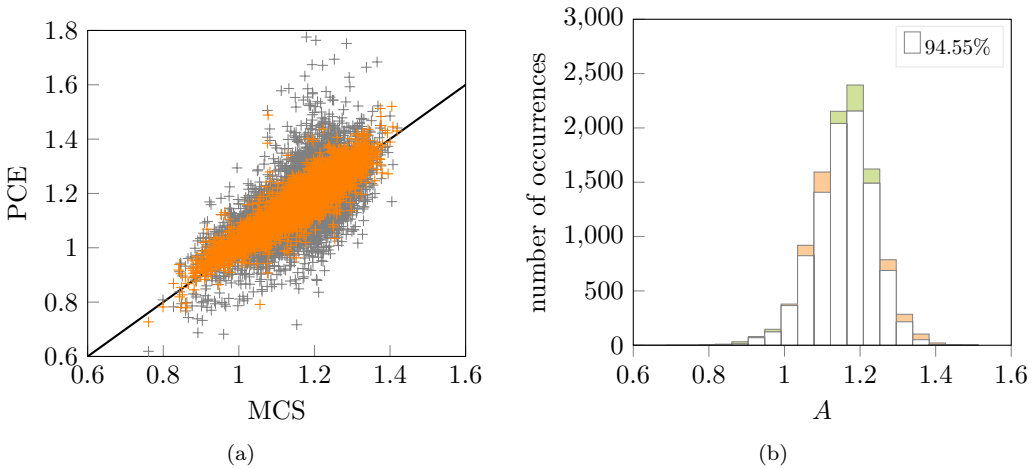

Figure 13. New PCE approximation of A by maximum of A_i ($q = 3$ and $n = 572$). (a) scatter plots of the previous PCE approximation (+) and the new PCE approximation (+); (b) PDF of A (■).

4.2.3 CI-PCE approximation

In comparison to PCE, CI-PCE advantageously allows to consider a reduced number of evaluations of the system response. Thus, while the degree remains $q = 3$, only $n_e = 58$ points are considered, which corresponds to the integer upper bound approximation of n/m_s. The CI-PCE approximation (■) of the system response over $N = 10\,000$ random samples is superimposed to Monte Carlo simulations (■) in Fig. 14.

For both quantities of interest, it is noticeable that CI-PCE yields results very close to those obtained with PCE: PDFs obtained with MCS and CI-PCE are almost perfectly superimposed while CI-PCE requires about ten times less evaluations of the system response. The minor increase in terms of intersection ratios from Figs. 12(a) and 13(b) to Fig. 14 is assumed to be related to the fact that the integer upper bound approximation of the required number of evaluations (58 instead of $n/m_s = 57.2$) was considered. One may note that $n_e = 58$ is significantly lower than the required minimum number of evaluations for standard PCE $p + 1 = 286$.

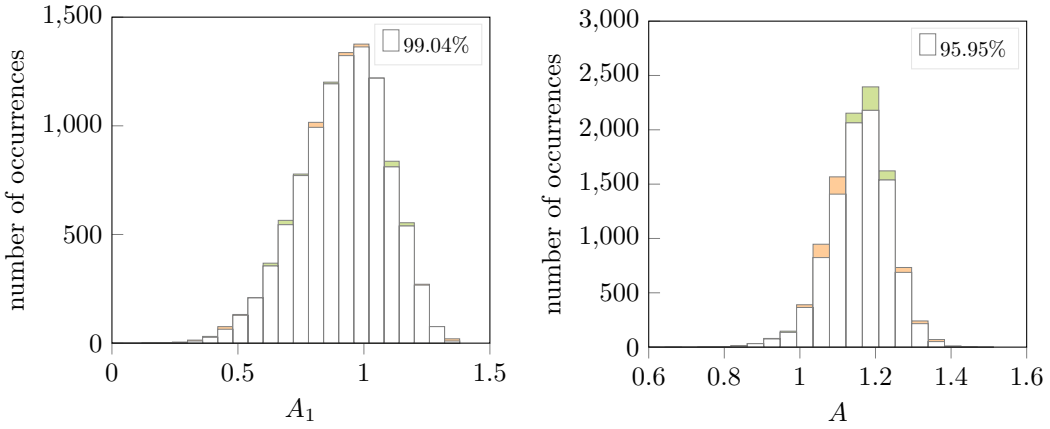

Figure 14. PDF of A and A_1 by MCS (■) and CI-PCE (■) ($q = 3$ and $n_e = 58$). (a) amplitude magnification of the first blade; (b) amplitude magnification of the bladed disk.

4.2.4 Partial conclusion

The confrontation of PCE and CI-PCE on a simple bladed disk model underlines the suitability of both methods for the prediction of amplitude magnifications. More particularly, the presented results show that PCE and CI-PCE are similarly accurate with respect to MCS. However, CI-PCE advantageously allows to decrease the number of required evaluations by a factor m_s, thus providing a very significant gain in terms of computational cost. Alternately, CI-PCE could also be seen as an efficient way to increase the accuracy of PCE results for a given computational cost, this is illustrated in the following section.

4.3 Industrial finite element model of a bladed disk

In this section, CI-PCE is applied to the 3D industrial finite element model of an aircraft engine compressor stage. Two quantities of interest are evaluated: (1) the bladed disk's first family of eigenfrequencies (related to the blades first bending mode), denoted $\{f_i\}_{i=1,m_s}$, and (2) the amplitude magnification, denoted A, defined in Eq. (44).

4.3.1 Model parameters and mistuning modeling

The industrial bladed disk model, which finite element mesh is depicted in Fig. 15, belongs to an aircraft engine compressor stage. The mesh and mechanical parameters of this model are detailed in Tab. 2. Within a stochastic framework, computations of the bladed disk's eigenfrequencies or magnitude amplification on the full finite element model would lead to unacceptable computation times. This motivates the use of component mode synthesis techniques in order to reduce the dimension of the model while accurately capturing its vibration behavior over a wide frequency range. The reduction procedure is twofold: a Craig-Bampton [63] modal reduction is first carried out before the component mode mistuning method [64] is employed to introduce mistuning in the system.

Mistuning is here represented by a variation of each blade Young's modulus E_i:

$$E_i = E_b(1 + \delta_i),\ i \in [\![1, m_s]\!], \tag{48}$$

where E_b is the nominal Young's modulus. It is assumed that the Young's modulus variation of each blade follows a uniform distribution over $[-\delta E, +\delta E]$. The mistuning standard deviation, referred to as the mistuning level, is defined by:

$$\sigma_E = \frac{2\delta E}{\sqrt{12}}. \tag{49}$$

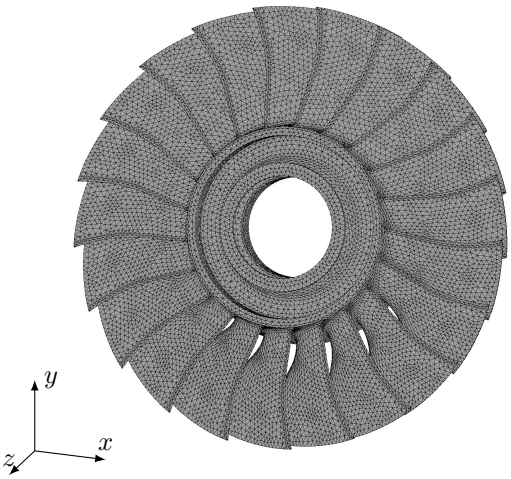

Figure 15. Finite element mesh for the industrial bladed disk.

description	value	unit
number of blades (m_s)	21	-
nominal Young's modulus (E_b)	2.1×10^{11}	Pa
damping ratio	10^{-2}	-
Poisson's ratio	0.3	-
amplitude of forcing	100	N
number of stator vanes	2	-
density	7850	$\mathrm{kg\,m^{-3}}$
blade length at leading edge	9.4×10^{-2}	m
disk radius	7.9×10^{-2}	m
number of elements per blade	9199	-
number of elements per sector	17 487	-

Table 2. Parameters of the industrial bladed disk model.

$\delta E(\%)$	0.25	0.5	0.75	1	2	3	4
$\sigma_E(\%)$	0.14	0.29	0.43	0.58	1.15	1.73	2.31

Table 3. Mistuning levels σ_E studied.

In the following, seven mistuning levels, see Tab. 3 are considered. All calculations are confronted to a reference approximation computed by MCS with $N = 10\,000$ random samples per mistuning level.

For each quantity of interest, preliminary investigations for PCE application have been conducted to determine the most suitable DoE and degree q while ensuring a low computational cost. For the sake of brevity, these preliminary investigations are not detailed in this article, nevertheless they led to conclude that a random points DoE combined with a low degree PCE (2 or 3) yielded accurate results with a reasonable computational cost. Standard PCE is thus carried out considering a degree $q = 2$, yielding $p + 1 = 253$ terms in the PCE basis. The DoE is composed of the minimum required number evaluations: it contains $p + 1$ random points. CI-PCE is applied with

the same degree $q = 2$, the elementary DoE contains $p + 1$ random points.

4.3.2 Eigenfrequencies

PCE and CI-PCE approximations of the bladed disk's eigenfrequencies computed for $N = 10\,000$ random samples are thereafter compared to MCS. For the sake of readability, only the results related to the first eigenfrequency, denoted f_1, are presented in the following. Results obtained for other eigenfrequencies of the structure's first modal family yield similar conclusions.

The PDF of f_1 obtained with PCE and CI-PCE, for a mistuning level $\sigma_E = 2.31\%$, are respectively depicted in Figs 16(a) and 16(b). The correlation coefficients between the MCS results, PCE and CI-PCE are given for all mistuning levels in Tab. 4. For a given mistuning level, the computational costs are 48.89 s for PCE, 48.96 s for

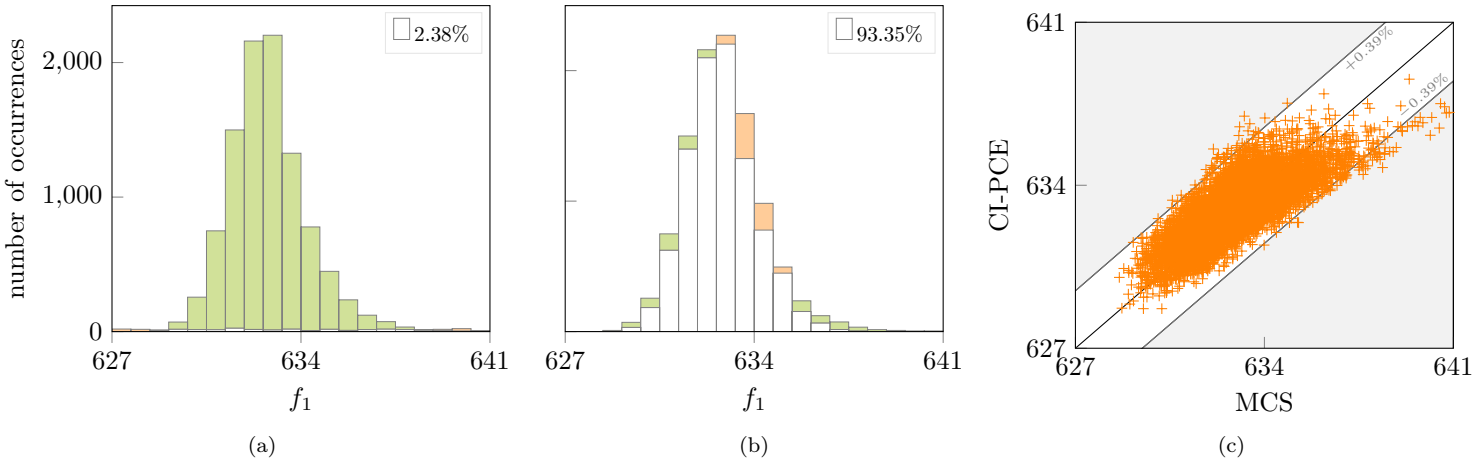

Figure 16. Approximation of f_1 by MCS (■) and PCE and CI-PCE for $\sigma_E = 2.31\%$ ($q = 2$ and 253 evaluations). (a) PDF of f_1 by PCE (■); (b) PDF of f_1 by CI-PCE (■); (c) scatter plot of the CI-PCE approximation (+).

$\sigma_E(\%)$	0.14	0.29	0.43	0.58	1.15	1.73	2.31
PCE	0.5809	0.1908	0.0865	0.0841	0.0896	−0.0327	−0.0337
CI-PCE	0.9999	0.9988	0.9949	0.9878	0.9289	0.8515	0.7816

Table 4. Correlation coefficients between the approximation of f_1 by MCS and respectively PCE and CI-PCE as a function of σ_E ($q = 2$ and 253 evaluations).

CI-PCE, and 2012.97 s for MCS. While CI-PCE uses the same evaluations as the ones used for PCE, it is noticeable that the CI-PCE results are significantly improved for all mistuning levels. Indeed, the correlation coefficient of f_1 increases between PCE and CI-PCE for all values of σ_E. In order to compare results sample per sample, the scatter plot of the 10 000 samples obtained by CI-PCE are compared to MCS results in Fig. 16(c). It is found that 99% of the samples obtained by CI-PCE feature a relative error lower than 0.39%.

In conclusion, these results highlight that CI-PCE yields significant gains in terms of accuracy in comparison to standard PCE while keeping an identical computational cost.

4.3.3 Amplitude magnification: first investigation

PCE and CI-PCE approximations of the bladed disk's amplitude magnification computed for $N = 10\,000$ random samples are thereafter compared to MCS following a two-step approach. In all cases, the degree of PCE and CI-PCE is $q = 2$. For this first investigation, PCE parameters used in the previous section are considered: the DoE comprises $n = p + 1 = 253$ random points, which corresponds to the theoretical minimum number of points that may be

used. Simultaneously, CI-PCE is applied considering the same number $n_e = p + 1 = 253$ of random points in the elementary DoE.

Depending on mistuning level, the 90th (-△-), 50th (-□-) and 10th (-○-) percentiles of the results of A obtained by MCS (——), PCE and CI-PCE (——) are depicted in Figs. 17(a) and 17(b). The correlation coefficients between MCS results, PCE and CI-PCE are given for all mistuning levels in Tab. 5. While CI-PCE relies on the same evaluations as the ones used for PCE, it is noticeable that the CI-PCE results are significantly improved, for all mistuning levels, in comparison to those obtained with PCE. For a given mistuning level, computational times (-●-) are plotted alongside relative computation times for the model preparation (left bar) and evaluation of the $N = 10\,000$ random samples (right bar) in Fig. 17(c). It is found that, contrary to MCS, the computational cost of PCE and CI-PCE is mostly related to the model preparation. Because of the dimension of the industrial model, the numerical cost of the additional operations required by CI-PCE (90 ms) is here negligible with respect to the computational cost of PCE so that both CI-PCE and PCE require identical computation times.

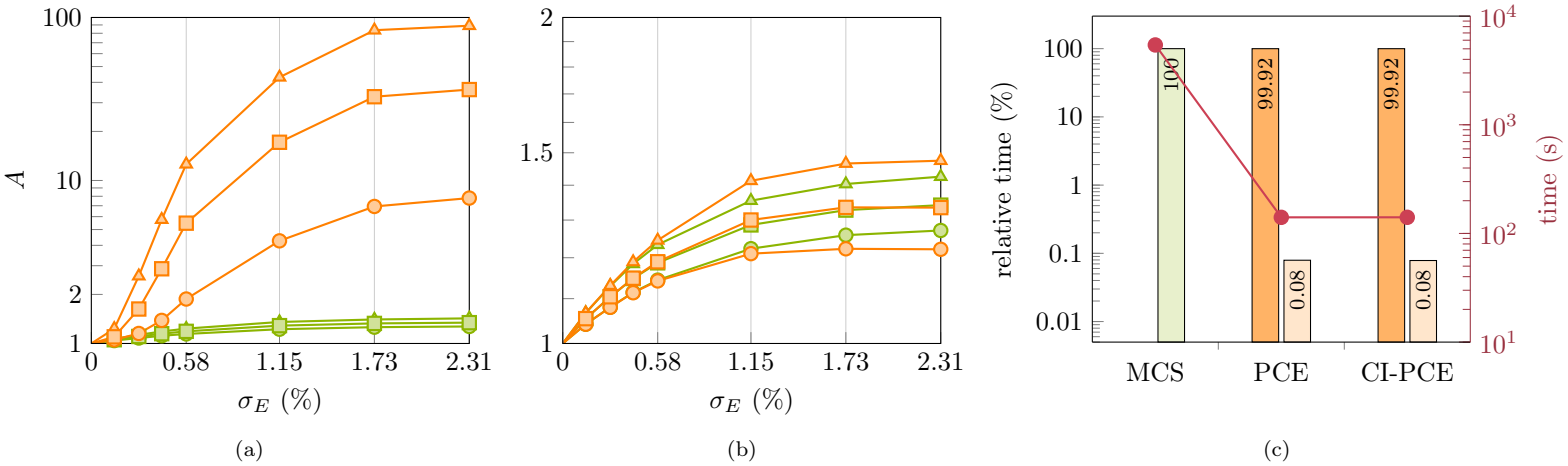

Figure 17. Approximation of A: 90th (-△-), 50th (-□-) and 10th (-○-) percentiles, and associated computation times. (a) PCE, $q = 2$, $n = 253$ (——) and MCS (——); (b) CI-PCE, $q = 2$, $n_e = 253$ (——) and MCS (——); (c) computation times (-●-), relative cost of the model preparation (■■) and samples evaluations (□□).

$\sigma_E(\%)$	0.14	0.29	0.43	0.58	1.15	1.73	2.31
PCE	0.1539	0.1019	0.1037	0.0794	0.0404	0.0174	0.0214
CI-PCE	0.9999	0.9982	0.9921	0.9776	0.8303	0.5798	0.4003

Table 5. Correlation coefficients between the approximation of A by MCS and respectively PCE and CI-PCE as a function of σ_E ($q = 2$ and 253 evaluations).

Overall, the computational cost for CI-PCE and PCE is more than one order of magnitude lower than MCS. Similarly to what was evidenced for the eigenfrequencies study, these results highlight that CI-PCE yields significant improvements in terms of accuracy in comparison to standard PCE while keeping an identical computational cost.

4.3.4 Amplitude magnification: second investigation

In this section, in order to improve the quality of the approximation, PCE is applied with a DoE comprising $n = 2(p + 1) = 506$ random points. At the same time, CI-PCE is applied with only $n_e = 25$ random points in the elementary DoE which correspond to the integer upper bound approximation of n/m_s. As in Fig. 17, PCE results and CI-PCE results are depicted in Figs. 18(a) and 18(b), respectively, along with the associated computational

times in Fig. 18(c). The correlation coefficients are given in Tab. 6. While CI-PCE requires only 25 evaluations compared to 506 for PCE, it is noticeable that CI-PCE yields results in very good agreement with those obtained with PCE. The computational times to evaluate the 10 000 samples are significantly reduced by CI-PCE: 13.93 s for CI-PCE, 274.23 s for PCE and 5427.81 s for MCS. Thus, these results confirm that CI-PCE is as accurate as PCE while advantageously requiring a much lower number $n_e = 25$ of the system response evaluations. One may note that $n_e = 25$ is also significantly lower than the required minimum number of evaluations for standard PCE $p + 1 = 253$.

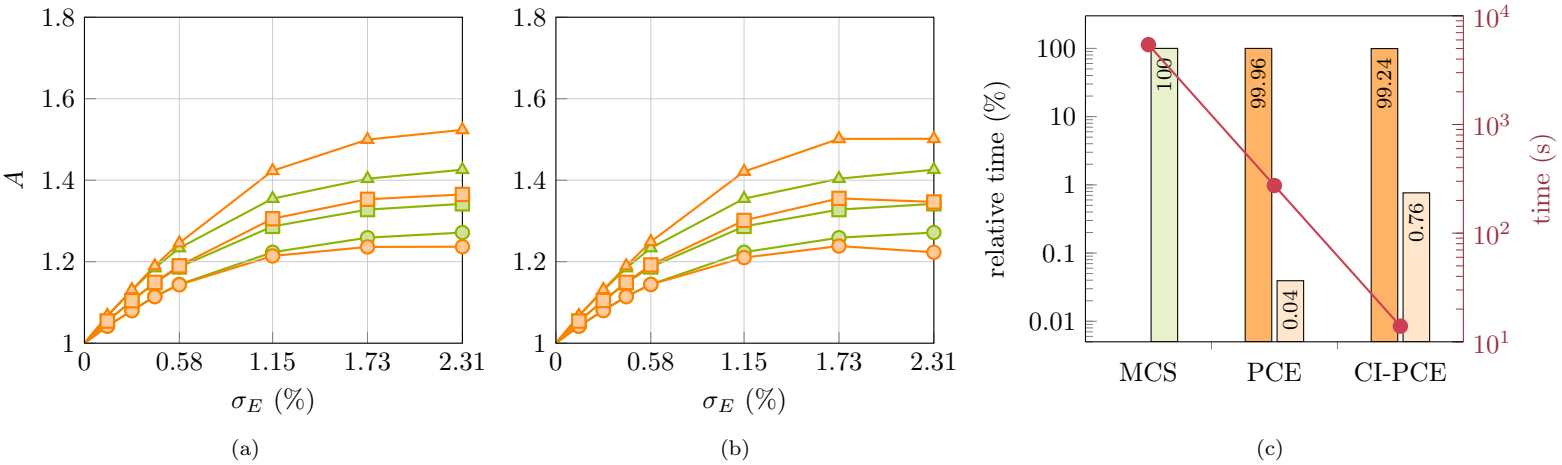

Figure 18. Approximation of A: 90th (-△-), 50th (-□-) and 10th (-○-) percentiles, and associated computation times. (a) PCE, $q = 2$, $n = 506$ (——) and MCS (——); (b) CI-PCE, $q = 2$, $n_e = 25$ (——) and MCS (——); (c) computation times (-●-), relative cost of the model preparation (■■) and samples evaluations (□□)

$\sigma_E(\%)$	0.14	0.29	0.43	0.58	1.15	1.73	2.31
PCE	0.9999	0.9982	0.9922	0.9785	0.8357	0.5877	0.4155
CI-PCE	0.9998	0.9967	0.9843	0.9551	0.7627	0.4865	0.3794

Table 6. Correlation coefficients between the approximation of f_1 by MCS and respectively PCE and CI-PCE as a function of σ_E ($q = 2$ and 506 evaluations for PCE and 25 for CI-PCE).

4.3.5 Partial conclusion

The confrontation of PCE and CI-PCE on an industrial bladed disk model underlines the potential of CI-PCE as it allows to obtain significantly more accurate results than the standard PCE for the prediction of both eigenfrequencies and amplitude magnification with identical computation times. Alternately, CI-PCE may be seen as a powerful way to reduce computational times as it only requires a number of evaluations m_s times lower than the one required for PCE, to reach the same level of accuracy obtained with PCE.

5 Conclusion

This work focuses on an improvement of the non-intrusive Polynomial Chaos Expansion dedicated to the stochastic analysis of cyclically symmetric engineering systems. The proposed developments (CI-PCE) are first introduced within a general mathematical framework, focusing on permutation invariant and cyclic permutation invariant functions. Analytical test functions featuring such properties are used to illustrate how the proposed developments allow to lower the computational cost of PCE by significantly reducing the required number of evaluations to build

the polynomial expansion. Should the number of evaluations be kept constant between PCE and CI-PCE, it is then underlined that the use of CI-PCE yields a significant improvement in terms of accuracy.

While reducing the number of required evaluations to a single elementary subspace of the random space is the cornerstone of the proposed developments, this is totally transparent for the end-user: CI-PCE is non-intrusive and applicable with any set of points belonging to the random space. It is also compatible with any sampling method that may be considered to define the design of experiments. This makes CI-PCE ready to use for industrial applications, should the investigated system be cyclic permutation invariant.

CI-PCE is finally applied in the context of turbomachinery to assess the influence of mistuning on bladed disks in terms of their eigenfrequencies or amplitude magnification. Two distinct types of bladed disks are considered: (1) a simple lumped mass model that was previously used in the literature, and for which reference results have thus been published, is first used for the sake of validation. Then, (2) a full 3D finite element model of an industrial compressor stage bladed disk is considered to demonstrate the computational efficiency of the proposed methodology. Both applications allow to underline that in comparison to PCE, CI-PCE yields significant improvements, be it in terms of results accuracy or overall computational cost. These applications also show that in the context of turbomachinery, a minor tweak of the proposed methodology allows to approximate quantities that are not cyclic permutation invariants such as a given blade amplitude magnification.

Acknowledgment

This research was undertaken thanks to funding from the Canada Research Chairs Program.

A Proof of Theorem 1

Proof 1. *For the case* (i)*, it may first be noted that Definition 2 leads to:*

$$\Omega_{\sigma,l} = \bigcap_{k=1}^{m_s-1} \underbrace{\{\boldsymbol{\xi} \in \Omega \,|\, 0 \leq f_k(\xi_1, \xi_2, \ldots, \xi_m)\}}_{C_k}, \tag{50}$$

where each polynomial function f_k *is defined by:*

$$\begin{aligned} f_k \colon \mathbb{R}^m &\to \mathbb{R} \\ (x_1, x_2, \ldots, x_m) &\mapsto x_{\sigma(k+1),l} - x_{\sigma(k),l}. \end{aligned}$$

Then, C_k *may be expressed as:*

$$C_k = f_k^{-1}([0, +\infty[), \forall k \in [\![1, m_s - 1]\!], \tag{51}$$

where $[0, +\infty[$ *is a closed set and* f_k *is continuous, this implies that* C_k *is a closed set. Additionally, the random variables* $\boldsymbol{\xi}$ *are bounded. Therefore,* C_k *is compact because it is both closed and bounded. Thus, it can be concluded that* $\Omega_{\sigma,l}$ *is compact by the intersection of compact sets.*

For the case (ii)*, considering* $(\mathbf{x}, \mathbf{y}) \in \Omega_{\sigma,l}$ *and* $\alpha \in [0, 1]$*, Definition 2 yields:*

$$\begin{cases} \mathbf{x} = (x_1, x_2, \ldots, x_m) \in \Omega \;\; \textit{such as} \;\; \forall k \in [\![1, m_s - 1]\!], \; x_{\sigma(k),l} \leq x_{\sigma(k+1),l}, & (52) \\ \mathbf{y} = (y_1, y_2, \ldots, y_m) \in \Omega \;\; \textit{such as} \;\; \forall k \in [\![1, m_s - 1]\!], \; y_{\sigma(k),l} \leq y_{\sigma(k+1),l}. & (53) \end{cases}$$

Let $k \in [\![1, m_s - 1]\!]$ *be an index, we have:*

$$\begin{cases} 0 \leq x_{\sigma(k+1),l} - x_{\sigma(k),l}, \\ 0 \leq y_{\sigma(k+1),l} - y_{\sigma(k),l}, \\ 0 \leq \alpha, \\ 0 \leq 1 - \alpha. \end{cases} \tag{54}$$

As a consequence:

$$0 \leq (1-\alpha)[x_{\sigma(k+1),l} - x_{\sigma(k),l}] + \alpha[y_{\sigma(k+1),l} - y_{\sigma(k),l}], \tag{55}$$

which can be rewritten as:

$$(1-\alpha)x_{\sigma(k),l} + \alpha y_{\sigma(k),l} \leq (1-\alpha)x_{\sigma(k+1),l} + \alpha y_{\sigma(k+1),l}. \tag{56}$$

Let $\mathbf{z} = (1-\alpha)\mathbf{x} + \alpha\mathbf{y}$*, the above equation can be written as:*

$$z_{\sigma(k),l} \leq z_{\sigma(k+1),l}. \tag{57}$$

Thus, $\mathbf{z} = (1-\alpha)\mathbf{x} + \alpha\mathbf{y} \in \Omega_{\sigma,l}$ *and it can be concluded that* $\Omega_{\sigma,l}$ *is convex.*

For the case (iii), $\Omega_{\sigma,l}$ *is a compact convex based on (i) and (ii). This implies that the boundary of* $\Omega_{\sigma,l}$ *is a null set.*

B Proof of Theorem 2

Proof 2. *From Theorem 1, we observe that* $\Omega_{\sigma_1,l} \bigcap \Omega_{\sigma_2,l}$ *is also a compact convex. Thus, we can conclude, by the property of a boundary of compact convex, that the boundary of* $\Omega_{\sigma_1,l} \bigcap \Omega_{\sigma_2,l}$ *is a null set.*

C Proof of Theorem 3

Proof 3. *From Theorem 1, we observe that the union on* $\sigma \in S_{m_s}$ *of the boundary of* $\Omega_{\sigma,l}$ *is a null set. Since the boundary of the union of* $\Omega_{\sigma,l}$ *is included in the union of boundaries of* $\Omega_{\sigma,l}$*, we can conclude that the boundary of* $\bigcup_{\sigma \in S_{m_s}} \Omega_{\sigma,l}$ *is a null set.*

D Proof of Theorem 4

Proof 4. *Let* σ *be a permutation of* S_{m_s} *and* $l \in [\![1, d]\!]$ *be an index so that* $\Omega_{\sigma,l}$ *denotes an elementary subspace of* Ω*. Let* $\boldsymbol{\xi}$ *be a point of* Ω*. Two cases must be distinguished:* $\boldsymbol{\xi} \in \Omega_{\sigma,l}$ *and* $\boldsymbol{\xi} \notin \Omega_{\sigma,l}$*.*

First, the case where $\boldsymbol{\xi} \in \Omega_{\sigma,l}$ *is considered, the elementary DoE* $\Xi_{\sigma,l}$ *may then be built in such a way that* $\boldsymbol{\xi} \in \Xi_{\sigma,l}$ *which yields* $\boldsymbol{\xi} \in \Xi$ *by Definition 4.*

In the case where $\boldsymbol{\xi} \notin \Omega_{\sigma,l}$*, there exists a sequence of distinct integers:*

$$(k_1, \ldots, k_r, k_{r+1}, \ldots, k_{m_s-1}) \in [\![1, m_s - 1]\!], \tag{58}$$

with $1 \leq r \leq m_s - 1$*, such that* $\boldsymbol{\xi}$ *does not satisfy Eq. (20):*

$$\begin{cases} \forall i \in [\![1, r]\!], & \xi_{\sigma(k_i),l} > \xi_{\sigma(k_i+1),l}, \\ \forall j \in [\![r+1, m_s - 1]\!], & \xi_{\sigma(k_j),l} \leq \xi_{\sigma(k_j+1),l}. \end{cases} \tag{59}$$

Let $\hat{\sigma}$ *be a permutation of* S_{m_s} *defined by:*

$$\begin{cases} \forall i \in [\![1, r]\!], & \hat{\sigma}(k_i) = k_i + 1, \\ \forall i \in [\![1, r]\!], & \hat{\sigma}(k_i + 1) = k_i, \\ \forall j \in [\![r+1, m_s - 1]\!], & \hat{\sigma}(k_j) = k_j, \\ & \hat{\sigma}(k_{m_s-1} + 1) = k_{m_s-1} + 1. \end{cases} \tag{60}$$

For the sake of readability, the notation $\mathbf{a} = \boldsymbol{\xi}^{(\hat{\sigma})}$ *is employed:*

$$a_{k,l} = \xi_{\hat{\sigma}(k),l}\ ,\ k \in [\![1, m_s - 1]\!]. \tag{61}$$

The permutation of $\mathbf{a}$ *by* σ *is:*

$$a_{\sigma(k),l} = \xi_{\sigma(\hat{\sigma}(k)),l}\ ,\ k \in [\![1, m_s - 1]\!]. \tag{62}$$

Based on Eq. (59), $\mathbf{a}$ *satisfies:*

$$\begin{cases} \forall i \in [\![1, r]\!], & a_{\sigma(k_i),l} = \xi_{\sigma(k_i+1),l} < \xi_{\sigma(k_i),l} = a_{\sigma(k_i+1),l}, \\ \forall j \in [\![r+1, m_s - 1]\!], & a_{\sigma(k_j),l} \leq a_{\sigma(k_j+1),l}. \end{cases} \tag{63}$$

Thus, $\mathbf{a} \in \Omega_{\sigma,l}$ *as defined in Eq. (20). Then,* $\Xi_{\sigma,l}$ *is built in such a way that* $\mathbf{a} \in \Xi_{\sigma,l}$ *which yields* $\mathbf{a}^{(\hat{\sigma}^{-1})} = \boldsymbol{\xi} \in \Xi$.

E Proof of Theorem 5

Proof 5. *From definition 4, the cardinal of* Ξ *is:*

$$|\Xi| \leq \sum_{\hat{\sigma} \in S_{m_s}} |\{\ \boldsymbol{\xi}^{(\hat{\sigma})}\ , \forall \boldsymbol{\xi} \in \Xi_{\sigma,l}\}| = m_s! n_e, \tag{64}$$

with equality if the sets $C_{\hat{\sigma}} = \{\ \boldsymbol{\xi}^{(\hat{\sigma})}\ , \forall \boldsymbol{\xi} \in \Xi_{\sigma,l}\}$ *are disjoint. It must be demonstrated that the sets* $C_{\hat{\sigma}}$ *are disjoint if and only if the points of* $\Xi_{\sigma,l}$ *are selected from the interior of* $\Omega_{\sigma,l}$.

Let $\hat{\sigma}_1$ *and* $\hat{\sigma}_2$ *be two distinct permutations of* S_{m_s}. *From Definition 2, it comes:*

$$C_{\hat{\sigma}_1} \cap C_{\hat{\sigma}_2} = \{\ \boldsymbol{\xi} \in \Xi_{\sigma,l}\,|\,\forall k \in [\![1, m_s]\!], \xi_{\hat{\sigma}_1(k),l} = \xi_{\hat{\sigma}_2(k),l}\} = \{\ \boldsymbol{\xi} \in \partial\Omega_{\sigma,l}\}, \tag{65}$$

where $\partial\Omega_{\sigma,l}$ *denotes the boundary of* $\Omega_{\sigma,l}$ *defined by:*

$$\partial\Omega_{\sigma,l} = \bigcup_{k=1}^{m_s-1} \{\boldsymbol{\xi} \in \Omega_{\sigma,l}\,|\,\xi_{\sigma(k),l} = \xi_{\sigma(k+1),l}\}, \tag{66}$$

which yields:

$$C_{\hat{\sigma}_1} \cap C_{\hat{\sigma}_2} = \emptyset \Leftrightarrow \Xi_{\sigma,l} = \{\boldsymbol{\xi}^{(j)} \in \Omega_{\sigma,l},\ |\ \boldsymbol{\xi}^{(j)} \notin \partial\Omega_{\sigma,l},\ j = 1, \ldots, n_e\}. \tag{67}$$

Thus, it can be concluded that the sets $C_{\hat{\sigma}}$ *are disjoint if and only if the points of* $\Xi_{\sigma,l}$ *are selected in the interior of* $\Omega_{\sigma,l}$ *and* $|\Xi| = m_s! n_e$.

F Proof of Theorem 6

Proof 6. *Let* $\boldsymbol{\xi}$ *be a point of* Ξ. *Analogously to Eq. (3), the evaluations of the polynomials of the PCE basis on* $\boldsymbol{\xi}$ *is defined by:*

$$\forall \boldsymbol{\alpha} \in \mathcal{A}, \quad \Psi_{\boldsymbol{\alpha}}(\boldsymbol{\xi}) = \prod_{k=1}^{m_s} \left(\prod_{h=1}^{d} \Phi_{\alpha_{k,h}}(\xi_{k,h}) \right). \tag{68}$$

From definition 4, there is a permutation $\hat{\sigma} \in S_{m_s}$ *such that* $\boldsymbol{\xi}^{(\hat{\sigma})} \in \Xi_{\sigma,l}$. *Then, by the variable change:*

$$k = \hat{\sigma}(\hat{k}),\ k \in \{1, \ldots, m_s\}, \tag{69}$$

the evaluation $\Psi_{\boldsymbol{\alpha}}(\boldsymbol{\xi})$ *can be rewritten as:*

$$\forall \boldsymbol{\alpha} \in \mathcal{A}, \quad \Psi_{\boldsymbol{\alpha}}(\boldsymbol{\xi}) = \prod_{\hat{k}=1}^{m_s} \left(\prod_{h=1}^{d} \Phi_{\alpha_{\hat{\sigma}(\hat{k}),h}}(\xi_{\hat{\sigma}(\hat{k}),h}) \right), \tag{70}$$

since $\hat{\sigma}^{-1}$ *is also a permutation* $\{1, 2, \dots, m_s\}$ *into* $\{1, 2, \dots, m_s\}$. *It may then be concluded that:*

$$\forall \boldsymbol{\alpha} \in \mathcal{A}, \quad \Psi_{\boldsymbol{\alpha}}(\boldsymbol{\xi}) = \Psi_{\boldsymbol{\alpha}^{(\hat{\sigma})}}(\boldsymbol{\xi}^{(\hat{\sigma})}), \tag{71}$$

where $\boldsymbol{\alpha}^{(\hat{\sigma})} = [\boldsymbol{\alpha}_1^{(\hat{\sigma})}, \dots, \boldsymbol{\alpha}_{m_s}^{(\hat{\sigma})}]$ *refers to the permutation of the multi-index* $\boldsymbol{\alpha}$ *for* $\hat{\sigma}$*:*

$$\alpha_{k,h}^{(\hat{\sigma})} = \alpha_{\hat{\sigma}(k),h}, \forall k \in [\![1, m_s]\!], \forall h \in [\![1, d]\!]. \tag{72}$$

References

[1] Corral, R., Khemiri, O., and Martel, C., 2018. "Design of mistuning patterns to control the vibration amplitude of unstable rotor blades". *Aerosp. Sci. Technol.,* **80**, pp. 20–28. doi: 10.1016/j.ast.2018.06.034.

[2] Panunzio, A. M., Salles, L., Schwingshackl, C., and Gola, M., 2015. "Asymptotic Numerical Method and Polynomial Chaos Expansion for the Study of Stochastic Non-Linear Normal Modes". In ASME Turbo Expo 2015: Turbine Technical Conference and Exposition, Vol. 7B: Structures and Dynamics. doi: 10.1115/GT2015-43560, oai: hal-02543866.

[3] Benini, E., and Biollo, R., 2007. "Aerodynamics of swept and leaned transonic compressor-rotors". *Appl. Energy,* **84**(10), pp. 1012–1027. doi: 10.1016/j.apenergy.2007.03.003.

[4] Castanier, M. P., and Pierre, C., 2006. "Modeling and analysis of mistuned bladed disk vibration: current status and emerging directions". *J. Propul. Power,* **22**(2), pp. 384–396. doi: 10.2514/1.16345.

[5] Legrand, M., Batailly, A., Magnain, B., Cartraud, P., and Pierre, C., 2012. "Full three-dimensional investigation of structural contact interactions in turbomachines". *J. Sound Vib.,* **331**(11), pp. 2578–2601. doi: 10.1016/j.jsv.2012.01.017, oai: hal-00660863.

[6] Beirow, B., Figaschewsky, F., Kühhorn, A., and Bornhorn, A., 2019. "Vibration analysis of an axial turbine blisk with optimized intentional mistuning pattern". *J. Sound Vib.,* **442**, pp. 11–27. doi: 10.1016/j.jsv.2018.10.064, oai: hal-02397955.

[7] Carassale, L., Cavicchi, A., Bruzzone, S., and Marrè Brunenghi, M., 2019. "Probabilistic Response of a Bladed Disk With Uncertain Geometry". *J. Eng. Gas Turbines Power,* **141**(10), p. . doi: 10.1115/1.4044642.

[8] Ewins, D., 1969. "The effects of detuning upon the forced vibrations of bladed disks". *J. Sound Vib.,* **9**(1), pp. 65–79. doi: 10.1016/0022-460X(69)90264-8.

[9] Hodges, C., 1982. "Confinement of vibration by structural irregularity". *J. Sound Vib.,* **82**(3), pp. 411–424. doi: 10.1016/S0022-460X(82)80022-9.

[10] Pierre, C., 1988. "Mode localization and eigenvalue loci veering phenomena in disordered structures". *J. Sound Vib.,* **126**(3), pp. 485–502. doi: 10.1016/0022-460X(88)90226-X.

[11] Whitehead, D. S., 1966. "Effect of mistuning on the vibration of turbo-machine blades induced by wakes". *J. Mech. Eng. Sci.,* **8**(1), pp. 15–21. doi: 10.1243/JMES_JOUR_1966_008_004_02.

[12] Óttarsson, G., and Pierre, C., 1995. "On the effects of interblade coupling on the statistics of maximum forced response amplitudes in mistuned bladed disks". In 36th Structures, Structural Dynamics and Materials Conference. doi: 10.2514/6.1995-1494.

[13] Óttarsson, G., and Pierre, C., 1993. "A Transfer Matrix Approach to Vibration Localization in Mistuned Blade Assemblies". In ASME International Gas Turbine and Aeroengine Congress and Exposition. doi: 10.1115/93-GT-115.

[14] Panning, L., Sextro, W., and Popp, K., 2002. "Optimization of the Contact Geometry Between Turbine Blades and Underplatform Dampers With Respect to Friction Damping". In ASME Turbo Expo 2002: Power for Land, Sea, and Air, Vol. 4: Turbo Expo 2002, Parts A and B, pp. 991–1002. doi: 10.1115/GT2002-30429.

[15] Laxalde, D., Thouverez, F., Sinou, J.-J., and Lombard, J.-P., 2007. "Qualitative analysis of forced response of blisks with friction ring dampers". *Eur. J. Mech. A. Solids,* **26**(4), pp. 676–687. doi: 10.1016/j.euromechsol.2006.10.002, oai: hal-00218249.

[16] Griffin, J. H., and Hoosac, T. M., 1984. "Model Development and Statistical Investigation of Turbine Blade Mistuning". *J. Vib., Acoust., Stress, and Reliab.,* **106**(2), pp. 204–210. doi: 10.1115/1.3269170.

[17] Choi, B.-K., Lentz, J., Rivas-Guerra, A. J., and Mignolet, M. P., 2002. "Optimization of Intentional Mistuning Patterns for the Reduction of the Forced Response Effects of Unintentional Mistuning: Formulation and Assessment". *J. Eng. Gas Turbines Power,* **125**(1), pp. 131–140. doi: 10.1115/1.1498270.

[18] Wei, S.-T., and Pierre, C., 1988. "Localization Phenomena in Mistuned Assemblies with Cyclic Symmetry Part II: Forced Vibrations". *J. Vib., Acoust., Stress, and Reliab,* **110**(4), pp. 439–449. doi: 10.1115/1.3269548.

[19] Rivas-Guerra, A. J., and Mignolet, M. P., 2004. "Local/Global Effects of Mistuning on the Forced Response of Bladed Disks". *J. Eng. Gas Turbines Power,* **126**(1), pp. 131–141. doi: 10.1115/1.1581898.

[20] Capiez-Lernout, E., Soize, C., Lombard, J.-P., Dupont, C., and Seinturier, E., 2005. "Blade Manufacturing Tolerances Definition for a Mistuned Industrial Bladed Disk ". *J. Eng. Gas Turbines Power,* **127**(3), pp. 621–628. doi: 10.1115/1.1850497, oai: hal-00686185.

[21] Wan, H.-P., Mao, Z., Todd, M. D., and Ren, W.-X., 2014. "Analytical uncertainty quantification for modal frequencies with structural parameter uncertainty using a gaussian process metamodel". *Eng. Struct.,* **75**, pp. 577–589. doi: 10.1016/j.engstruct.2014.06.028.

[22] Wan, H.-P., Ren, W.-X., and Todd, M. D., 2017. "An efficient metamodeling approach for uncertainty quantification of complex systems with arbitrary parameter probability distributions". *Int. J. Numer. Methods Eng.,* **109**(5), pp. 739–760. doi: 10.1002/nme.5305.

[23] Ghanem, R. G., and Spanos, P. D., 1991. *Stochastic finite elements: a spectral approach.* Springer, New York, NY. doi: 10.1007/978-1-4612-3094-6.

[24] Wiener, N., 1938. "The Homogeneous Chaos". *American Journal of Mathematics,* **60**(4), pp. 897–936. doi: 10.2307/2371268.

[25] Sudret, B., and Der Kiureghian, A., 2000. Stochastic Finite Element Methods and Reliability A State-of-the-Art Report. Tech. Rep. UCB/SEMM-2000/08, Department of Civil and Environmental Engineering, University of California, Berkeley.

[26] Berveiller, M., Sudret, B., and Lemaire, M., 2006. "Stochastic finite element: a non intrusive approach by regression". *Eur. J. Comp. Mech.,* **15**(1-3), pp. 81–92. doi: 10.3166/remn.15.81-92, oai: hal-01665506.

[27] Philippe, J., Thouverez, F., Blanc, L., and Gruin, M., 2018. "Vibratory behavior prediction of mistuned stator vane clusters: An industrial application". *Comput. Struct.,* **196**, pp. 12–23. doi: 10.1016/j.compstruc.2017.11.003.

[28] Wan, H.-P., Ren, W.-X., and Todd, M. D., 2020. "Arbitrary polynomial chaos expansion method for uncertainty quantification and global sensitivity analysis in structural dynamics". *Mech. Syst. Sig. Process.,* **142**, p. 106732. doi: 10.1016/j.ymssp.2020.106732.

[29] Bladh, R., Castanier, M. P., and Pierre, C., 1999. "Reduced Order Modeling and Vibration Analysis of Mistuned Bladed Disk Assemblies With Shrouds". *J. Eng. Gas Turbines Power,* **121**(3), pp. 515–522. doi: 10.1115/1.2818503.

[30] Legrand, M., Batailly, A., and Pierre, C., 2011. "Numerical investigation of abradable coating removal in aircraft engines through plastic constitutive law". *J. Comput. Nonlinear Dyn.,* **7**(1), p. . doi: 10.1115/1.4004951, oai: hal-00627526.

[31] Petrov, E. P., 2012. "Multiharmonic Analysis of Nonlinear Whole Engine Dynamics With Bladed Disc-Casing Rubbing Contacts". In ASME Turbo Expo 2012: Turbine Technical Conference and Exposition, Vol. 7: Structures and Dynamics, Parts A and B, pp. 1181–1191. doi: 10.1115/GT2012-68474.

[32] Panning, L., Popp, K., Sextro, W., Götting, F., Kayser, A., and Wolter, I., 2004. "Asymmetrical Underplatform Dampers in Gas Turbine Bladings: Theory and Application". In ASME Turbo Expo 2004: Power for Land, Sea, and Air, Vol. 6: Turbo Expo 2004, pp. 269–280. doi: 10.1115/GT2004-53316.

[33] Firrone, C. M., Zucca, S., and Gola, M., 2011. "The effect of underplatform dampers on the forced response of bladed disks by a coupled static/dynamic harmonic balance method". *Int. J. Non Linear Mech.,* **46**(2), pp. 363–375. doi: 10.1016/j.ijnonlinmec.2010.10.001.

[34] Salles, L., Blanc, L., Thouverez, F., and Gouskov, A., 2011. "Dynamic analysis of fretting-wear in friction contact interfaces". *Int. J. Solids Struct.,* **48**(10), pp. 1513–1524. doi: 10.1016/j.ijsolstr.2011.01.035.

[35] Legrand, M., Pierre, C., Cartraud, P., and Lombard, J.-P., 2009. "Two-dimensional modeling of an aircraft engine structural bladed disk-casing modal interaction". *J. Sound Vib.,* **319**(1-2), pp. 366–391. doi: 10.1016/j.jsv.2008.06.019, oai: hal-00328186.

[36] Parent, M.-O., Thouverez, F., and Chevillot, F., 2014. "Whole Engine Interaction in a Bladed Rotor-to-Stator Contact". In ASME Turbo Expo 2014: Turbine Technical Conference and Exposition, Vol. 7A: Structures and Dynamics. doi: 10.1115/GT2014-25253, oai: hal-01223063.

[37] Ma, H., Tai, X., Han, Q., Wu, Z., Wang, D., and Wen, B., 2015. "A revised model for rubbing between rotating blade and elastic casing". *J. Sound Vib.,* **337**, pp. 301–320. doi: 10.1016/j.jsv.2014.10.020, oai: hal-01430515.

[38] Jacquet-Richardet, G., Torkhani, M., Cartraud, P., Thouverez, F., Baranger, T. N., Herran, M., Gibert, C., Baguet, S., Almeida, P., and Peletan, L., 2013. "Rotor to stator contacts in turbomachines. review and application". *Mech. Syst. Sig. Process.,* **40**(2), pp. 401–420. doi : 10.1016/j.ymssp.2013.05.010, oai: hal-00934050.

[39] Joachim, J., Nyssen, F., and Batailly, A., 2020. "Numerical investigation of a mistuned academic bladed disk dynamics with blade/casing contact". *J. Eng. Gas Turbines Power*, p. . doi: 10.1115/1.4047780, oai: hal-02896893.

[40] Le Maître, O. P., Reagan, M. T., Najm, H. N., Ghanem, R. G., and Knio, O. M., 2002. "A Stochastic Projection Method for Fluid Flow: II. Random Process". *J. Comput. Phys.,* **181**(1), pp. 9–44. doi: 10.1006/jcph.2002.7104.

[41] Rajasekharan-Nair, R., and Petrov, E., 2018. "Analysis of Deformation of Mistuned Bladed Disks With Friction and Random Crystal Anisotropy Orientation Using Gradient-Based Polynomial Chaos Expansion". *J. Eng. Gas Turbines Power,* **141**(4), p. . doi: 10.1115/1.4040906.

[42] Wan, X., and Karniadakis, G. E., 2005. "An adaptive multi-element generalized polynomial chaos method for stochastic differential equations". *J. Comput. Phys.,* **209**(2), pp. 617–642. doi: 10.1016/j.jcp.2005.03.023.

[43] Sarrouy, E., Dessombz, O., and Sinou, J.-J., 2013. "Piecewise polynomial chaos expansion with an application to brake squeal of a linear brake system". *J. Sound Vib.,* **332**(3), pp. 577–594. doi: 10.1016/j.jsv.2012.09.009, oai: hal-00744841.

[44] Blatman, G., and Sudret, B., 2008. "Sparse polynomial chaos expansions and adaptive stochastic finite elements using a regression approach". *C. R. Mécanique,* **336**(6), pp. 518–523. doi: 10.1016/j.crme.2008.02.013.

[45] Marelli, S., and Sudret, B., 2018. "An active-learning algorithm that combines sparse polynomial chaos expansions and bootstrap for structural reliability analysis". *Struct. Saf.,* **75**, pp. 67–74. doi: 10.1016/j.strusafe.2018.06.003, oai: hal-01902018.

[46] Sinha, A., 2005. "Computation of the Statistics of Forced Response of a Mistuned Bladed Disk Assembly via Polynomial Chaos". *J. Vib. Acoust.,* **128**(4), pp. 449–457. doi: 10.1115/1.2215620.

[47] Cameron, R. H., and Martin, W. T., 1947. "The Orthogonal Development of Non-Linear Functionals in Series of Fourier-Hermite Functionals". *Ann. Math.,* **48**(2), pp. 385–392. doi: 10.2307/1969178.

[48] Xiu, D., and Karniadakis, G. E., 2002. "The Wiener-Askey polynomial chaos for stochastic differential equations". *SIAM J. Sci. Comput.,* **24**(2), pp. 619–644. doi: 10.1137/S1064827501387826.

[49] Blatman, G., and Sudret, B., 2011. "Adaptive sparse polynomial chaos expansion based on least angle regression". *J. Comput. Phys.,* **230**(6), pp. 2345–2367. doi: 10.1016/j.jcp.2010.12.021.

[50] Le Maître, O. P., and Knio, O. M., 2010. *Spectral methods for uncertainty quantification: with applications to computational fluid dynamics*. Springer Science & Business Media. doi: 10.1007/978-90-481-3520-2.

[51] Sudret, B., 2008. "Global sensitivity analysis using polynomial chaos expansions". *Reliab. Eng. Syst. Saf.,* **93**(7), pp. 964–979. doi: 10.1016/j.ress.2007.04.002.

[52] Klema, V., and Laub, A., 1980. "The singular value decomposition: Its computation and some applications". *IEEE Trans. Autom. Control,* **25**(2), pp. 164–176. doi: 10.1109/TAC.1980.1102314.

[53] Morokoff, W. J., and Caflisch, R. E., 1994. "Quasi-Random Sequences and Their Discrepancies". *SIAM J. Sci. Comput.,* **15**, pp. 1251–1279. doi: 10.1137/0915077.

[54] Blatman, G., Sudret, B., and Berveiller, M., 2007. "Quasi random numbers in stochastic finite element analysis". *Mech. Ind.,* **8**(3), p. 289–297. doi: 10.1051/meca:2007051.

[55] Gao, Z., and Zhou, T., 2014. "On the Choice of Design Points for Least Square Polynomial Approximations with Application to Uncertainty Quantification". *Comm. Comput. Phys.,* **16**(2), p. 365–381. doi: 10.4208/cicp.130813.060214a.

[56] Webster, M. D., Tatang, M. A., and McRae, G. J., 1996. Application of the probabilistic collocation method for an uncertainty analysis of a simple ocean model. Tech. Rep. 4, MIT Joint Program on the Science and Policy of Global Change, Massachusetts Institute of Technology.

[57] Isukapalli, S. S., 1999. "Uncertainty analysis of transport-transformation models". phdthesis, The State University of New Jersey, New Brunswick Rutgers.

[58] Zein, S., Colson, B., and Glineur, F., 2013. "An Efficient Sampling Method for Regression-Based Polynomial Chaos Expansion". *Comm. Comput. Phys.,* **13**(4), p. 1173–1188. doi: 10.4208/cicp.020911.200412a.

[59] Hadigol, M., and Doostan, A., 2018. "Least squares polynomial chaos expansion: A review of sampling strategies". *Comput. Methods Appl. Mech. Engrg,* **332**, pp. 382–407. doi: 10.1016/j.cma.2017.12.019.

[60] Crestaux, T., Le Maître, O. P., and Martinez, J.-M., 2009. "Polynomial chaos expansion for sensitivity analysis". *Reliab. Eng. Syst. Saf.,* **94**(7), pp. 1161–1172. doi: 10.1016/j.ress.2008.10.008.

[61] Yuan, J., Scarpa, F., Allegri, G., Titurus, B., Patsias, S., and Rajasekaran, R., 2017. "Efficient computational techniques for mistuning analysis of bladed discs: A review". *Mech. Syst. Sig. Process.,* **87**, pp. 71–90. doi: 10.1016/j.ymssp.2016.09.041.

[62] Szepietowska, K., Magnain, B., Lubowiecka, I., and Florentin, E., 2018. "Sensitivity analysis based on non-intrusive regression-based polynomial chaos expansion for surgical mesh modelling". *Struct. Multidiscip. Optim.,* **57**(3), pp. 1391–1409. doi: 10.1007/s00158-017-1799-9, oai: hal-02060949.

[63] Craig, R. R., and Bampton, M. C. C., 1968. "Coupling of Substructures for Dynamic Analyses". *AIAA Journal,* **6**(7), pp. 1313–1319. doi: 10.2514/3.4741, oai: hal-01537654.

[64] Lim, S.-H., Bladh, R., Castanier, M. P., and Pierre, C., 2007. "Compact, generalized component mode mistuning representation for modeling bladed disk vibration". *AIAA Journal,* **45**(9), pp. 2285–2298. doi: 10.2514/1.13172.